

Harmonic decomposition of three-particle azimuthal correlations at RHIC

L. Adamczyk,¹ J. K. Adkins,¹⁹ G. Agakishiev,¹⁷ M. M. Aggarwal,³¹ Z. Ahammed,⁵⁰ N. N. Ajitanand,⁴⁰ I. Alekseev,^{15,26} D. M. Anderson,⁴² R. Aoyama,⁴⁶ A. Aparin,¹⁷ D. Arkhipkin,³ E. C. Aschenauer,³ M. U. Ashraf,⁴⁵ A. Attri,³¹ G. S. Averichev,¹⁷ X. Bai,⁷ V. Bairathi,²⁷ A. Behera,⁴⁰ R. Bellwied,⁴⁴ A. Bhasin,¹⁶ A. K. Bhati,³¹ P. Bhattarai,⁴³ J. Bielcik,¹⁰ J. Bielcikova,¹¹ L. C. Bland,³ I. G. Bordyuzhin,¹⁵ J. Bouchet,¹⁸ J. D. Brandenburg,³⁶ A. V. Brandin,²⁶ D. Brown,²³ I. Bunzarov,¹⁷ J. Butterworth,³⁶ H. Caines,⁵⁴ M. Calderón de la Barca Sánchez,⁵ J. M. Campbell,²⁹ D. Cebra,⁵ I. Chakaberia,³ P. Chaloupka,¹⁰ Z. Chang,⁴² N. Chankova-Bunzarova,¹⁷ A. Chatterjee,⁵⁰ S. Chattopadhyay,⁵⁰ X. Chen,³⁷ J. H. Chen,³⁹ X. Chen,²¹ J. Cheng,⁴⁵ M. Cherney,⁹ W. Christie,³ G. Contin,²² H. J. Crawford,⁴ S. Das,⁷ L. C. De Silva,⁹ R. R. Debbé,³ T. G. Dedovich,¹⁷ J. Deng,³⁸ A. A. Derevschikov,³³ L. Didenko,³ C. Dilks,³² X. Dong,²² J. L. Drachenberg,²⁰ J. E. Draper,⁵ L. E. Dunkelberger,⁶ J. C. Dunlop,³ L. G. Efimov,¹⁷ N. Elsey,⁵² J. Engelage,⁴ G. Eppley,³⁶ R. Esha,⁶ S. Esumi,⁴⁶ O. Evdokimov,⁸ J. Ewigleben,²³ O. Eyster,³ R. Fatemi,¹⁹ S. Fazio,³ P. Federic,¹¹ P. Federicova,¹⁰ J. Fedorisin,¹⁷ Z. Feng,⁷ P. Filip,¹⁷ E. Finch,⁴⁷ Y. Fisyak,³ C. E. Flores,⁵ L. Fulek,¹ C. A. Gagliardi,⁴² D. Garand,³⁴ F. Geurts,³⁶ A. Gibson,⁴⁹ M. Girard,⁵¹ D. Grosnick,⁴⁹ D. S. Gunarathne,⁴¹ Y. Guo,¹⁸ A. Gupta,¹⁶ S. Gupta,¹⁶ W. Guryn,³ A. I. Hamad,¹⁸ A. Hamed,⁴² A. Harlenderova,¹⁰ J. W. Harris,⁵⁴ L. He,³⁴ S. Heppelmann,³² S. Heppelmann,⁵ A. Hirsch,³⁴ G. W. Hoffmann,⁴³ S. Horvat,⁵⁴ T. Huang,²⁸ B. Huang,⁸ X. Huang,⁴⁵ H. Z. Huang,⁶ T. J. Humanic,²⁹ P. Huo,⁴⁰ G. Igo,⁶ W. W. Jacobs,¹⁴ A. Jentsch,⁴³ J. Jia,^{3,40} K. Jiang,³⁷ S. Jowzaee,⁵² E. G. Judd,⁴ S. Kabana,¹⁸ D. Kalinkin,¹⁴ K. Kang,⁴⁵ K. Kauder,⁵² H. W. Ke,³ D. Keane,¹⁸ A. Kechechyan,¹⁷ Z. Khan,⁸ D. P. Kikola,⁵¹ I. Kisel,¹² A. Kisiel,⁵¹ L. Kochenda,²⁶ M. Kocmanek,¹¹ T. Kollegger,¹² L. K. Kosarzewski,⁵¹ A. F. Kraishan,⁴¹ P. Kravtsov,²⁶ K. Krueger,² N. Kulathunga,⁴⁴ L. Kumar,³¹ J. Kvapil,¹⁰ J. H. Kwasizur,¹⁴ R. Lacey,⁴⁰ J. M. Landgraf,³ K. D. Landry,⁶ J. Lauret,³ A. Lebedev,³ R. Lednicky,¹⁷ J. H. Lee,³ X. Li,³⁷ C. Li,³⁷ W. Li,³⁹ Y. Li,⁴⁵ J. Lidrych,¹⁰ T. Lin,¹⁴ M. A. Lisa,²⁹ H. Liu,¹⁴ P. Liu,⁴⁰ Y. Liu,⁴² F. Liu,⁷ T. Ljubicic,³ W. J. Llope,⁵² M. Lomnitz,²² R. S. Longacre,³ S. Luo,⁸ X. Luo,⁷ G. L. Ma,³⁹ L. Ma,³⁹ Y. G. Ma,³⁹ R. Ma,³ N. Magdy,⁴⁰ R. Majka,⁵⁴ D. Mallick,²⁷ S. Margetis,¹⁸ C. Markert,⁴³ H. S. Matis,²² K. Meehan,⁵ J. C. Mei,³⁸ Z. W. Miller,⁸ N. G. Minaev,³³ S. Mioduszewski,⁴² D. Mishra,²⁷ S. Mizuno,²² B. Mohanty,²⁷ M. M. Mondal,¹³ D. A. Morozov,³³ M. K. Mustafa,²² Md. Nasim,⁶ T. K. Nayak,⁵⁰ J. M. Nelson,⁴ M. Nie,³⁹ G. Nigmatkulov,²⁶ T. Niida,⁵² L. V. Nogach,³³ T. Nonaka,⁴⁶ S. B. Nurushev,³³ G. Odyniec,²² A. Ogawa,³ K. Oh,³⁵ V. A. Okorokov,²⁶ D. Olivitt Jr.,⁴¹ B. S. Page,³ R. Pak,³ Y. Pandit,⁸ Y. Panebratsev,¹⁷ B. Pawlik,³⁰ H. Pei,⁷ C. Perkins,⁴ P. Pile,³ J. Pluta,⁵¹ K. Poniatowska,⁵¹ J. Porter,²² M. Posik,⁴¹ A. M. Poskanzer,²² N. K. Pruthi,³¹ M. Przybycien,¹ J. Putschke,⁵² H. Qiu,³⁴ A. Quintero,⁴¹ S. Ramachandran,¹⁹ R. L. Ray,⁴³ R. Reed,²³ M. J. Rehbein,⁹ H. G. Ritter,²² J. B. Roberts,³⁶ O. V. Rogachevskiy,¹⁷ J. L. Romero,⁵ J. D. Roth,⁹ L. Ruan,³ J. Rusnak,¹¹ O. Rusnakova,¹⁰ N. R. Sahoo,⁴² P. K. Sahu,¹³ S. Salur,²² J. Sandweiss,⁵⁴ M. Saur,¹¹ J. Schambach,⁴³ A. M. Schmah,²² W. B. Schmidke,³ N. Schmitz,²⁴ B. R. Schweid,⁴⁰ J. Seger,⁹ M. Sergeeva,⁶ P. Seyboth,²⁴ N. Shah,³⁹ E. Shahaliev,¹⁷ P. V. Shanmuganathan,²³ M. Shao,³⁷ A. Sharma,¹⁶ M. K. Sharma,¹⁶ W. Q. Shen,³⁹ Z. Shi,²² S. S. Shi,⁷ Q. Y. Shou,³⁹ E. P. Sichtermann,²² R. Sikora,¹ M. Simko,¹¹ S. Singha,¹⁸ M. J. Skoby,¹⁴ N. Smirnov,⁵⁴ D. Smirnov,³ W. Solyst,¹⁴ L. Song,⁴⁴ P. Sorensen,³ H. M. Spinka,² B. Srivastava,³⁴ T. D. S. Stanislaus,⁴⁹ M. Strikhanov,²⁶ B. Stringfellow,³⁴ T. Sugiura,⁴⁶ M. Sumbera,¹¹ B. Summa,³² Y. Sun,³⁷ X. M. Sun,⁷ X. Sun,⁷ B. Surrow,⁴¹ D. N. Svirida,¹⁵ A. H. Tang,³ Z. Tang,³⁷ A. Taranenko,²⁶ T. Tarnowsky,²⁵ A. Tawfik,⁵³ J. Thäder,²² J. H. Thomas,²² A. R. Timmins,⁴⁴ D. Tlusty,³⁶ T. Todoroki,³ M. Tokarev,¹⁷ S. Trentalange,⁶ R. E. Tribble,⁴² P. Tribedy,³ S. K. Tripathy,¹³ B. A. Trzeciak,¹⁰ O. D. Tsai,⁶ T. Ullrich,³ D. G. Underwood,² I. Upsal,²⁹ G. Van Buren,³ G. van Nieuwenhuizen,³ A. N. Vasiliev,³³ F. Videbæk,³ S. Vokal,¹⁷ S. A. Voloshin,⁵² A. Vossen,¹⁴ G. Wang,⁶ Y. Wang,⁷ F. Wang,³⁴ Y. Wang,⁴⁵ J. C. Webb,³ G. Webb,³ L. Wen,⁶ G. D. Westfall,²⁵ H. Wieman,²² S. W. Wissink,¹⁴ R. Witt,⁴⁸ Y. Wu,¹⁸ Z. G. Xiao,⁴⁵ W. Xie,³⁴ G. Xie,³⁷ J. Xu,⁷ N. Xu,²² Q. H. Xu,³⁸ Y. F. Xu,³⁹ Z. Xu,³ Y. Yang,²⁸ Q. Yang,³⁷ C. Yang,³⁸ S. Yang,³ Z. Ye,⁸ Z. Ye,⁸ L. Yi,⁵⁴ K. Yip,³ I. -K. Yoo,³⁵ N. Yu,⁷ H. Zbroszczyk,⁵¹ W. Zha,³⁷ Z. Zhang,³⁹ X. P. Zhang,⁴⁵ J. B. Zhang,⁷ S. Zhang,³⁷ J. Zhang,²¹ Y. Zhang,³⁷ J. Zhang,²² S. Zhang,³⁹ J. Zhao,³⁴ C. Zhong,³⁹ L. Zhou,³⁷ C. Zhou,³⁹ X. Zhu,⁴⁵ Z. Zhu,³⁸ and M. Zyzak¹²

(STAR Collaboration)

¹AGH University of Science and Technology, FPACS, Cracow 30-059, Poland

²Argonne National Laboratory, Argonne, Illinois 60439

³Brookhaven National Laboratory, Upton, New York 11973

⁴University of California, Berkeley, California 94720

⁵University of California, Davis, California 95616

⁶University of California, Los Angeles, California 90095

- ⁷Central China Normal University, Wuhan, Hubei 430079
⁸University of Illinois at Chicago, Chicago, Illinois 60607
⁹Creighton University, Omaha, Nebraska 68178
¹⁰Czech Technical University in Prague, FNSPE, Prague, 115 19, Czech Republic
¹¹Nuclear Physics Institute AS CR, 250 68 Prague, Czech Republic
¹²Frankfurt Institute for Advanced Studies FIAS, Frankfurt 60438, Germany
¹³Institute of Physics, Bhubaneswar 751005, India
¹⁴Indiana University, Bloomington, Indiana 47408
¹⁵Alikhanov Institute for Theoretical and Experimental Physics, Moscow 117218, Russia
¹⁶University of Jammu, Jammu 180001, India
¹⁷Joint Institute for Nuclear Research, Dubna, 141 980, Russia
¹⁸Kent State University, Kent, Ohio 44242
¹⁹University of Kentucky, Lexington, Kentucky, 40506-0055
²⁰Lamar University, Physics Department, Beaumont, Texas 77710
²¹Institute of Modern Physics, Chinese Academy of Sciences, Lanzhou, Gansu 730000
²²Lawrence Berkeley National Laboratory, Berkeley, California 94720
²³Lehigh University, Bethlehem, PA, 18015
²⁴Max-Planck-Institut für Physik, Munich 80805, Germany
²⁵Michigan State University, East Lansing, Michigan 48824
²⁶National Research Nuclear University MEPhI, Moscow 115409, Russia
²⁷National Institute of Science Education and Research, Bhubaneswar 751005, India
²⁸National Cheng Kung University, Tainan 70101
²⁹Ohio State University, Columbus, Ohio 43210
³⁰Institute of Nuclear Physics PAN, Cracow 31-342, Poland
³¹Panjab University, Chandigarh 160014, India
³²Pennsylvania State University, University Park, Pennsylvania 16802
³³Institute of High Energy Physics, Protvino 142281, Russia
³⁴Purdue University, West Lafayette, Indiana 47907
³⁵Pusan National University, Pusan 46241, Korea
³⁶Rice University, Houston, Texas 77251
³⁷University of Science and Technology of China, Hefei, Anhui 230026
³⁸Shandong University, Jinan, Shandong 250100
³⁹Shanghai Institute of Applied Physics, Chinese Academy of Sciences, Shanghai 201800
⁴⁰State University Of New York, Stony Brook, NY 11794
⁴¹Temple University, Philadelphia, Pennsylvania 19122
⁴²Texas A&M University, College Station, Texas 77843
⁴³University of Texas, Austin, Texas 78712
⁴⁴University of Houston, Houston, Texas 77204
⁴⁵Tsinghua University, Beijing 100084
⁴⁶University of Tsukuba, Tsukuba, Ibaraki, Japan,
⁴⁷Southern Connecticut State University, New Haven, CT, 06515
⁴⁸United States Naval Academy, Annapolis, Maryland, 21402
⁴⁹Valparaiso University, Valparaiso, Indiana 46383
⁵⁰Variable Energy Cyclotron Centre, Kolkata 700064, India
⁵¹Warsaw University of Technology, Warsaw 00-661, Poland
⁵²Wayne State University, Detroit, Michigan 48201
⁵³World Laboratory for Cosmology and Particle Physics (WLCAPP), Cairo 11571, Egypt
⁵⁴Yale University, New Haven, Connecticut 06520

We present measurements of three-particle correlations for various harmonics in Au+Au collisions at energies ranging from $\sqrt{s_{\text{NN}}} = 7.7$ to 200 GeV using the STAR detector. The quantity $\langle \cos(m\phi_1 + n\phi_2 - (m+n)\phi_3) \rangle$ is evaluated as a function of $\sqrt{s_{\text{NN}}}$, collision centrality, transverse momentum, p_T , pseudo-rapidity difference, $\Delta\eta$, and harmonics (m and n). These data provide detailed information on global event properties like the three dimensional structure of the initial overlap region, the expansion dynamics of the matter produced in the collisions, and the transport properties of the medium. A strong dependence on $\Delta\eta$ is observed for most harmonic combinations consistent with breaking of longitudinal boost invariance. Data reveal changes with energy in the two-particle correlation functions relative to the second-harmonic event-plane and provide ways to constrain models of heavy-ion collisions over a wide range of collision energies.

I. INTRODUCTION

Heavy nuclei are collided at facilities like the Relativistic Heavy Ion Collider (RHIC) and the Large Hadron

Collider (LHC) in order to study the emergent properties of matter with quarks and gluons as the dominant degrees-of-freedom: a quark-gluon plasma (QGP) [1–4].

The QGP is a form of matter that existed in the early universe when its ambient temperature was more than 155 MeV or 200 thousand times hotter than the center of the sun [5, 6]. As temperatures drop, quarks and gluons no longer possess the energy necessary to overcome the confining forces of QCD and they become confined into color neutral hadrons and the QGP transitions smoothly and continuously into a gas of hadrons [7]. This transition occurred in the early universe at about one microsecond after the big bang. Heavy-ion collisions provide the only known method to recreate and study that phase transition in a laboratory setting.

To provide the clearest possible picture of this phase transition, a beam energy scan was carried out at RHIC with collision energies ranging from $\sqrt{s_{NN}}=200$ GeV down to 7.7 GeV. Lowering the beam energy naturally reduces the initial temperature of the matter created in the collisions providing information on how the transport properties and equilibrium of the matter vary with temperature [8]. These heavy-ion collisions however create systems that are both very small and short-lived. The characteristic size of the collision region is the size of a nucleus or approximately 10^{-14} meters across. This system expands in the longitudinal direction and eventually in the transverse direction so that the energy density drops quickly. Any quark gluon plasma that exists will only survive for on the order 5×10^{-23} seconds. Given the smallness of the system and its very brief lifetime, it is challenging to determine the nature of the matter left behind after the initial collisions. Physicists rely on indirect observations based on particles streaming from the collision region which are observed long after any QGP has ceased to exist. Correlations between these produced particles have provided insight into the early phases of the expansion as well as the characteristics of the matter undergoing the expansion [9]. The dependence of the correlations on the azimuthal angle between particles $\Delta\phi = \phi_1 - \phi_2$ has proven to be particularly informative. Data have revealed that even when particle pairs are separated by large angles in the longitudinal direction (large $\Delta\eta$), they remain strongly correlated in the azimuthal direction. This correlation manifests itself as a prominent ridge-like structure in two-particle, $\Delta\eta$, $\Delta\phi$, correlation functions [10]. The origin of this ridge has been traced to the initial geometry of the collision region where flux tubes are localized in the transverse direction but stretch over a long distance in the longitudinal direction [11–14]. How well these structures from the initial geometry are translated into correlations between particles emitted from the collision region reveals information about the medium’s viscosity: the larger the viscosity, the more washed out the correlations will become [15]. To study these effects, it is convenient to examine the coefficients of a Fourier transform of the $\Delta\phi$ dependence of the two-particle correlation functions [16]. These coefficients have been variously labeled as V_n , a_n , or $v_n^2\{2\}$ where n is the harmonic. Although the latter is perhaps more cumbersome, we have maintained its usage owing

to its connection to the original terminology used for two-particle cumulants which has been in use for more than a decade [17]. While $v_n^2\{2\} = \langle \cos n(\Delta\phi) \rangle$ has been studied as a function of $\sqrt{s_{NN}}$, centrality, harmonic n , p_T , and $\Delta\eta$ [18], in this paper we extend this analysis from two-particle correlations to three-particle mixed harmonic correlations of the form $\langle \cos(m\phi_1 + n\phi_2 - (m+n)\phi_3) \rangle$ [19] where m and n are positive integers.

Extending the analysis of azimuthal correlations from two to three particles provides several benefits. First, the three particle correlations provide greater sensitivity to the three-dimensional structure of the initial state by for example revealing information about the two-particle $\Delta\eta - \Delta\phi$ correlations with respect to the reaction plane. Many models of heavy-ion collisions make the simplifying assumption that the initial geometry of the collision overlap doesn’t vary with rapidity and that a boost invariant central rapidity plateau may be considered [20]. It is likely however that this assumption is broken by the asymmetric nature of the initial state and that precision comparisons between models and data will require a fuller understanding of the initial state fluctuations in all three dimensions [21]. Second, the new measurements can constrain models [22–25]. When signals seen in two-particle correlations may be mocked up by multiple effects, three-particle correlations can break those ambiguities. This is important as models become more sophisticated by including for example bulk viscosity, shear viscosity, and their temperature dependence [26]. Also, three-particle correlations can reveal information about how two-particle correlations change as a function of their angle with respect to the reaction plane. When one of the harmonics m , n , or $m+n$ is equal to two, that harmonic will be dominated by the preference of particles to flow in the direction of the reaction plane. This feature has been exploited to study charge separation relative to the reaction plane through measurements of the charge dependence of $\langle \cos(\phi_1 + \phi_2 - 2\phi_3) \rangle$ [27, 28]. The motivation for those measurements was to search for evidence of the chiral magnetic effect (CME) in heavy-ion collisions [29–31]. By extending the measurements to other harmonics we can ascertain more information about the nature of the correlations interpreted as evidence for CME. Finally, three-particle correlations reveal information about how various harmonics are correlated with each other. For example, Teaney and Yan [22] originally proposed the measurement of $\langle \cos(\phi_1 + 2\phi_2 - 3\phi_3) \rangle$ because initial state models predict a strong correlation between the first, second and third harmonics of the spatial density distribution. That correlation can be traced to collision geometries where a nucleon from one nucleus fluctuates toward the edge of that nucleus and impinges on the oncoming nucleus. This leads to something similar to a $p + A$ collision and a high density near the edge of the main collision region. That configuration increases the predicted v_3 by a factor of 2-3 in noncentral collisions so that v_3 deviates from the $1/\sqrt{N_{\text{part}}}$ one would expect from random fluctuations in the positions of the nucleons partic-

ipating in the collision [15, 16, 18]. That configuration should also be asymmetric in the forward and backward rapidity directions, again pointing to the importance of understanding the three dimensional structure of the initial state. If the evidence proposed by Teaney and Yan is not confirmed, then one may question the validity of any model that predicts the centrality dependence of v_n based on those initial condition models. In this paper we present measurements of $\langle \cos(m\phi_1 + n\phi_2 - (m+n)\phi_3) \rangle$ as a function of energy, centrality, $\Delta\eta$, p_T , and harmonics m and n . Data confirm the predicted correlation between the first, second and third harmonics but the $\Delta\eta$ dependence points to the potential importance of including the three-dimensional structure of the initial state in the model calculations.

In the following, we first describe the experiment and the analysis (Sec. II). We then present the results in Sec. III including the $\Delta\eta$ dependence (Sec. III A), the centrality dependence (Sec. III B), the p_T dependence (Sec. III C), and the beam energy dependence (Sec. III D). Conclusions are presented in Sec. IV. We include measurements of $v_n^2\{2\}$ for $n=1,2,4$, and 5 in the appendix.

II. EXPERIMENT AND ANALYSIS

Our measurements make use of data collected from Au+Au collisions with the STAR detector at RHIC in the years 2004, 2010, 2011, 2012, and 2014. The charged particles used in this analysis are detected through their ionization energy loss in the STAR Time Projection Chamber [32]. The transverse momentum p_T , η , and charge are determined from the trajectory of the track in STAR's solenoidal magnetic field. With the 0.5 Tesla field used during data taking, particles can be reliably tracked for $p_T > 0.2$ GeV/c. The efficiency for finding particles drops quickly as p_T decreases below this value [34]. Weights have been used to correct the three-particle correlation functions for the p_T -dependent efficiency and for imperfections in the detector acceptance. The quantity analyzed and reported is

$$C_{m,n,m+n} = \langle \cos(m\phi_1 + n\phi_2 - (m+n)\phi_3) \rangle = \left\langle \left(\frac{\sum_{i,j,k} w_i w_j w_k \cos(m\phi_i + n\phi_j + (m+n)\phi_k)}{\sum_{i,j,k} w_i w_j w_k} \right) \right\rangle \quad (1)$$

where $\langle \rangle$ represents an average over events and $\sum_{i,j,k}$ is a sum over unique particle triplets within an event. Each event is weighted by the number of unique triplets in that event. The weights $w_{i,j,k}$ are determined from the inverse of the ϕ distributions after they have been averaged over many events (which for a perfect detector should be flat) and by the p_T dependent efficiency. The $w_{i,j,k}$ depend on the particles' p_T , η , and charge and the collisions' centrality and z-vertex location. The correction procedure

is verified by checking that the ϕ distributions are flat after the correction so that $\langle \cos n(\phi) \rangle$ and $\langle \sin n(\phi) \rangle$ are near zero. With these corrections, the data represent the $C_{m,n,m+n}$ that would be seen by a detector with perfect acceptance for particles with $p_T > 0.2$ GeV/c and $|\eta| < 1$. In practice, calculating all possible combinations of three particles individually would be computationally too costly to be practical, particularly for the larger data sets at 200 GeV. In that case we use algebra based on Q-vectors ($Q_n = \sum \exp(in\phi)$) to reduce the computational challenge [33]. Differential measurements like the $\Delta\eta$ dependence of the correlations, however, require explicit calculations for at least two of the particles. Studying the $\Delta\eta$ dependence of the correlations also allows us to correct for the effect of track-merging on the correlations. Track-merging leads to a large anti-correlation between particle pairs that are close to each other in the detector. The effect becomes large in central collisions where the detector occupancy is largest. After weight corrections have been applied to correct for single particle acceptance effects, the effect of track-merging is the largest remaining correction. Data have been divided into standard centrality classes (0-5%, 5-10%, 10-20%,... 70-80%) based on the number of charged hadrons within $|\eta| < 0.5$ observed for a given event. In some figures, we will report the centrality in terms of the number of participating nucleons (N_{part}) estimated from a Monte Carlo Glauber calculations [34, 35].

The three-particle correlations presented in this paper are related to the low-resolution limit of the event-plane measurements that have been explored at the LHC [36]. Practically this would be carried out by dividing $C_{m,n,m+n}$ by $\langle v_m v_n v_{m+n} \rangle$. Typically, however, v_n is measured from a two-particle correlation function such as the two-particle cumulants $v_n = \sqrt{v_n^2\{2\}}$ or a similar measurement and the $v_n^2\{2\}$ are not positive-definite quantities. As such, $\sqrt{v_n^2\{2\}}$ can, and often does, become imaginary. This is particularly true for the first harmonic and also at lower collision energies. For this reason we report the pure three-particle correlations which, in any case, do not suffer from the ambiguities related to the low- and high-resolution limits associated with reaction plane analyses [19, 37] and are therefore easier to interpret theoretically.

III. RESULTS

In the following, we present the $\Delta\eta$ dependence of the three-particle correlations for several harmonic combinations corrected for track-merging. After removing the effects of track merging and Hanbury Brown and Twiss (HBT) correlations [38], we integrate over the $\Delta\eta$ dependence of the correlations and present the resulting integrated correlations as a function of centrality for the energies $\sqrt{s_{\text{NN}}}=200, 62.4, 39, 27, 19.6, 14.5, 11.5$, and 7.7 GeV. We also investigate the p_T dependence of the correlations by plotting them as a function of the p_T of

either the first or second particle used in the correlation. Finally, we study how the data depends on the beam energy.

A. $\Delta\eta$ Dependence

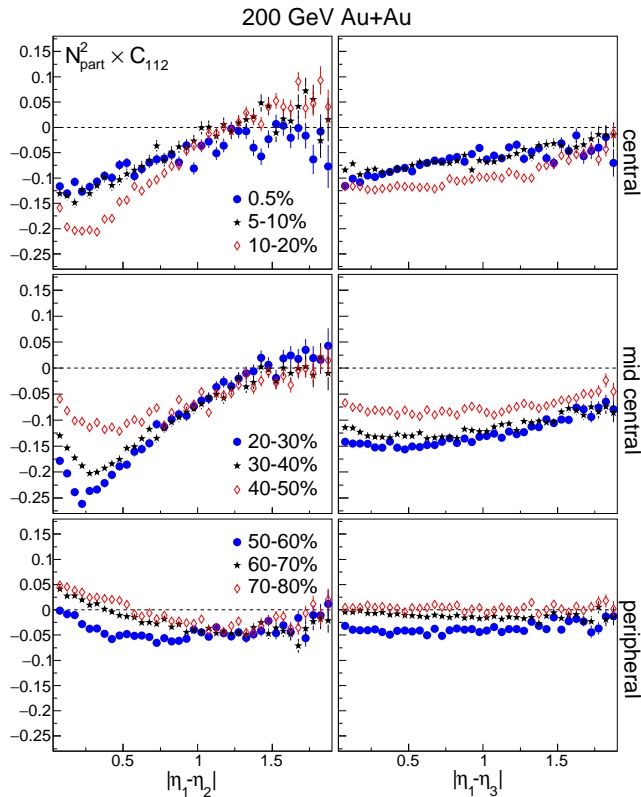


FIG. 1. (color online) The $\Delta\eta$ dependence of $C_{1,1,2}$ scaled by N_{part}^2 for 9 centrality intervals with the three most central classes shown in the top panels and the three most peripheral in the bottom. The N_{part} values used for the corresponding centralities are 350.6, 298.6, 234.3, 167.6, 117.1, 78.3, 49.3, 28.2 and 15.7. In the panels on the left, $\Delta\eta$ is taken between particles 1 and 2 while on the right it is between particles 1 and 3 (which is identical to 2 and 3). Data are from 200 GeV Au+Au collisions and for charged hadrons with $p_T > 0.2$ GeV/c, $|\eta| < 1$.

Figure 1 shows the $\Delta\eta$ dependence of $C_{1,1,2}$ scaled by N_{part}^2 for charged hadrons with $p_T > 0.2$ GeV/c and $|\eta| < 1$. The scaling accounts for the natural dilution of correlations expected if the more central collisions can be treated as a linear superposition of nucleon-nucleon collisions. Results for nine different centrality intervals from 200 GeV Au+Au collisions are shown. We do not include the uncertainty on N_{part} in the uncertainties in our figures. The left panels show the correlations as a function of the difference in η between the first and second particle. Note that the subscripts in $C_{m,n,m+n}$ refer to the harmonic number while the subscripts for the η

refers to the particle number. The right panels show the same but as a function of the difference between particles 1 and 3. The $C_{1,1,2}$ correlation is similar to the correlation used in the search for the chiral magnetic effect except that we do not separate out the cases when particles 1 and 2 have like-sign charges vs unlike-sign charges as is done when looking for charge separation with respect to the reaction plane. These measurements can be approximately related to the reaction-plane based measurements by scaling the three-particle correlations by $1/v_2$. We note that the difference in $C_{1,1,2}$ for different charge combinations is as large as the signal with $C_{1,1,2}$ being nearly zero for unlike-sign combinations of particle 1 and 2. This correlation may also be influenced by momentum conservation effects as well. It's not clear however how those effects would be distributed with respect to $\Delta\eta$.

In the left panels of Fig. 1, we see a strong dependence for $C_{1,1,2}$ on $|\eta_1 - \eta_2|$. In central collisions, the data starts out negative at the smallest values of $|\eta_1 - \eta_2|$ but then begins to increase and becomes close to zero or even positive near $|\eta_1 - \eta_2| = 1.5$. At small $|\eta_1 - \eta_2|$, a narrow peak is seen in the correlation that is related to HBT. As we progress from central to peripheral collisions, the trends change with $C_{1,1,2}$ in peripheral collisions exhibiting a positive value at small $|\eta_1 - \eta_2|$, perhaps signaling the dominance of jets in the correlation function in these peripheral collisions.

The left panels share the same scales as the right panels making it clear that the dependence of $C_{1,1,2}$ on $|\eta_1 - \eta_3|$ is much weaker than the dependence on $|\eta_1 - \eta_2|$. This is expected since the $e^{-2i\phi_3}$ term in $C_{1,1,2} = \langle e^{i\phi_1} e^{i\phi_2} e^{-2i\phi_3} \rangle$ will be dominated by the global preference of particles to be emitted in the direction of the reaction plane. For all but the most central collisions, the almond shaped geometry of the collision overlap region is approximately invariant with rapidity. This is not likely the case for other harmonics.

Figure 2 shows $C_{1,2,3}$ scaled by N_{part}^2 as a function of $|\eta_1 - \eta_2|$ (left panels) and $|\eta_1 - \eta_3|$ (right panels). In this case, $C_{1,2,3}$ exhibits a stronger dependence on $|\eta_1 - \eta_3|$ than on $|\eta_1 - \eta_2|$. The variation with $|\eta_2 - \eta_3|$ is very similar to the variation with $|\eta_1 - \eta_2|$ and is omitted from the figures to improve legibility. Again, the $e^{i2\phi_2}$ component of $C_{1,2,3}$ is dominated by the reaction plane which is largely invariant within the η range covered by these measurements so that $C_{1,2,3}$ depends very little on the η_2 , $|\eta_1 - \eta_2|$, or $|\eta_2 - \eta_3|$. However, $C_{1,2,3}$ depends very strongly on $|\eta_1 - \eta_3|$. This dependence may arise from the longitudinal asymmetry inherent in the fluctuations that lead to predictions for large values of $C_{1,2,3}$ [24]. In models for the initial geometry, the correlations are induced between the first, second, and third harmonics of the eccentricity by cases where a nucleon fluctuates towards the edge of the nucleus [39]. If that occurs in the reaction plane direction and towards the other nucleus in the collision, then that nucleon can collide with many nucleons from the other nucleus. This geometry will cause the first and third harmonics to become correlated with

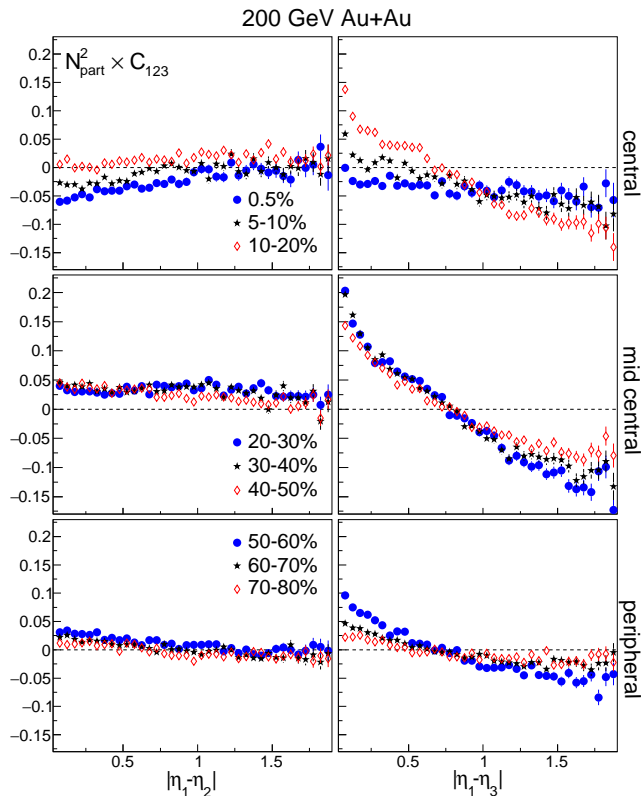


FIG. 2. (color online). The $\Delta\eta$ dependence of $C_{1,2,3}$ scaled by N_{part}^2 for 9 centrality intervals with the three most central classes shown in the top panels and the three most peripheral in the bottom. In the panels on the left, $\Delta\eta$ is taken between particles 1 and 2 while on the right it is between particles 1 and 3. Data are from 200 GeV Au+Au collisions and for charged hadrons with $p_T > 0.2$ GeV/c, $|\eta| < 1$.

the second harmonic. Since the collision of one nucleon from one nucleus with many nucleons in the other nucleus is asymmetric along the rapidity axis, we argue that we can expect a strong dependence on $|\eta_1 - \eta_3|$. Models that assume the initial energy density is symmetric with rapidity (boost invariant) will likely fail to describe this behavior. One may also speculate that the variation with $|\eta_1 - \eta_3|$ could arise from sources like jets or resonances particularly if they interact with the medium so that they become correlated with the reaction plane. Making use of the full suite of measurements provided here will help delineate between these two scenarios.

In Fig. 3 we present the $|\eta_1 - \eta_2|$ and $|\eta_1 - \eta_3|$ dependence of $C_{2,2,4}$. This correlation is more strongly influenced by the reaction plane correlations and exhibits much larger values than either $C_{1,1,2}$ or $C_{1,2,3}$. The dependence on $|\eta_1 - \eta_2|$ and $|\eta_1 - \eta_3|$ are also weaker with $C_{2,2,4}$ in central and mid-central collisions showing little variation over the $|\eta_1 - \eta_2|$ range, consistent with a mostly η -independent reaction plane within the measured range. A larger variation is observed with

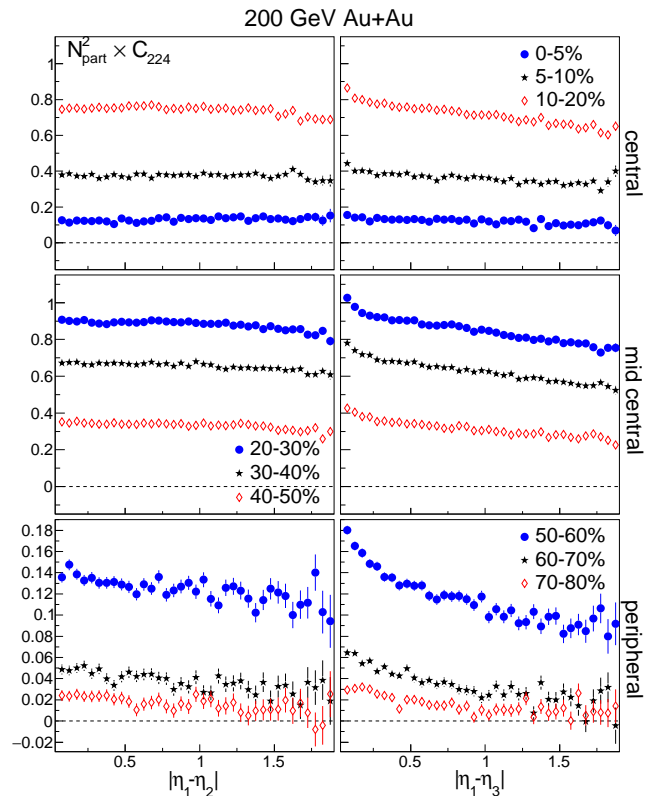


FIG. 3. (color online) The $\Delta\eta$ dependence of $C_{2,2,4}$ scaled by N_{part}^2 for 9 centrality intervals with the three most central classes shown in the top panels and the three most peripheral in the bottom. In the panels on the left, $\Delta\eta$ is taken between particles 1 and 2 while on the right it is between particles 1 and 3 (identical to 2 and 3). Data are from 200 GeV Au+Au collisions and for charged hadrons with $p_T > 0.2$ GeV/c, $|\eta| < 1$.

$|\eta_1 - \eta_3|$ which in mid-central collisions amounts to an approximately 20% variation. We also note that in mid-central collisions, the change in value of $C_{2,2,4}$ over the range $0 < |\eta_1 - \eta_3| < 2$ is similar in magnitude to the change of $C_{1,1,2}$ over $0 < |\eta_1 - \eta_2| < 2$ and $C_{1,2,3}$ over $0 < |\eta_1 - \eta_3| < 2$.

In Fig. 4 we present the $|\eta_1 - \eta_2|$ and $|\eta_2 - \eta_3|$ dependence of $C_{2,3,5}$. Again, $C_{2,3,5}$ only exhibits a weak dependence on $|\eta_1 - \eta_2|$ but a stronger dependence on $|\eta_2 - \eta_3|$. In central and mid-central collisions, a strong short-range correlation at $|\eta_2 - \eta_3| < 0.4$ is apparent consistent with HBT and Coulomb correlations that vary with respect to the reaction plane. In addition to that peak, $C_{2,3,5}$ decreases as $|\eta_2 - \eta_3|$ increases. Although the relative variation of $C_{2,3,5}$ is similar to $C_{2,2,4}$, the absolute change is much smaller than for $C_{1,1,2}$, $C_{1,2,3}$, or $C_{2,2,4}$.

The combination of the various $C_{m,n,m+n}$ can help elucidate the nature of the three-particle correlations. If the $|\eta_1 - \eta_3|$ dependence of $C_{1,2,3}$ arises from correlations between particles from jets correlated with the reaction

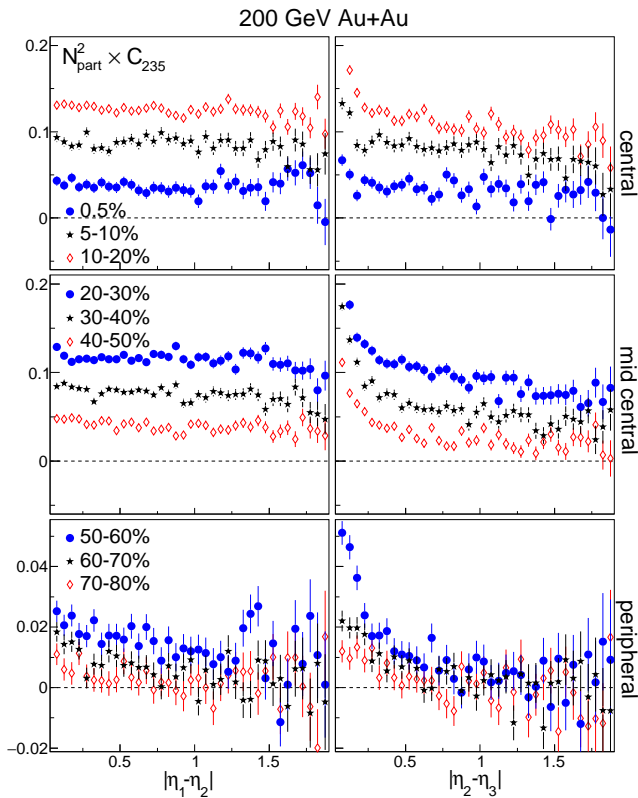


FIG. 4. (color online) The $\Delta\eta$ dependence of $C_{2,3,5}$ scaled by N_{part}^2 for 9 centrality intervals with the three most central classes shown in the top panels and the three most peripheral in the bottom. In the panels on the left, $\Delta\eta$ is taken between particles 1 and 2 while on the right it is between particles 1 and 3 (identical to 2 and 3). Data are from 200 GeV Au+Au collisions and for charged hadrons with $p_T > 0.2$ GeV/c, $|\eta| < 1$.

plane, we would expect the particles at small $\Delta\eta$ to predominantly come from the near-side jet (at $\Delta\phi \approx 0$) and particles at larger $\Delta\eta$ to come from the away-side jet (at $\Delta\phi \approx \pi$ radians). In that case, at small $\Delta\eta$, $C_{m,n,m+n}$ for all harmonics will have a positive contribution from the jets. The same is not true however for large $\Delta\eta$ where we would expect the correlations to be dominated by the away-side jet separated by π radians. For this case at large $\Delta\eta$, $C_{1,1,2}$ and $C_{1,2,3}$ would receive negative contributions from the away side jet while $C_{2,2,4}$ and $C_{2,3,5}$ would both receive positive contributions. The trends observed across the variety of $C_{m,n,m+n}$ measurements are inconsistent with this simple picture with $C_{2,2,4}$ decreasing by nearly the same amount as $C_{1,2,3}$ as $\Delta\eta$ is increased. A more complicated picture of the effect of jets would therefore be required to account for the observed data but it appears difficult to construct a non-flow scenario that can account for the long-range variation of $C_{m,n,m+n}$. Breaking of boost-invariance in the initial density distributions may provide an explanation for the observed variations but we do not know of any

specific model that has been shown to describe our data.

B. Centrality Dependence

In Figs. 5 and 6 we show $C_{m,n,m+n}$ correlations scaled by N_{part}^2 with $(m,n) = (1,1), (1,2), (1,3), (2,2), (2,3), (2,4), (3,3),$ and $(3,4)$ for $\sqrt{s_{\text{NN}}} = 200, 62.4, 39, 27, 19.6, 14.5, 11.5,$ and 7.7 GeV Au+Au collisions as a function of N_{part} . Data are for charged particles with $|\eta| < 1$ and $p_T > 0.2$ GeV/c. The correlation $C_{2,2,4}$, by far the largest of the measured correlations, has been scaled by a factor of 1/5. Otherwise, the scales on each of the three panels are kept the same for each energy to make it easier to compare the magnitudes of the different harmonic combinations.

At 200 GeV, $C_{1,1,2}$ is negative for all centralities except for the most peripheral where it is slightly positive but consistent with zero. $C_{1,2,3}$ is consistent with zero in peripheral collisions, positive in mid-central collisions but then becomes negative in central collisions. If the second and third harmonic event planes are uncorrelated, then $C_{1,2,3}$ should be zero. The $C_{1,2,3}$ correlation is non-zero deviating from that expectation. The magnitude is however much smaller than originally anticipated based on a linear hydrodynamic response to initial state geometry fluctuations [22]. Non-linear coupling between harmonics, where the fifth harmonic for example is dominated by a combination of the second and third harmonic, has been shown to be very important [23, 40]. In the case of $C_{1,2,3}$, the non-linear contribution has an opposite sign to the linear contribution and similar magnitude canceling out most of the expected strength of $C_{1,2,3}$. This suggests that $C_{1,2,3}$ is very sensitive to the nonlinear nature of the hydrodynamic model. $C_{1,3,4}$ is close to zero for all centralities indicating little or no correlation between the first, third, and fourth harmonics. The other $C_{m,n,m+n}$ correlations are positive for all centralities. When considering the comparison of this data to hydrodynamic models, it is important to also consider the strong $\Delta\eta$ dependence of the correlations as shown in the previous section.

The correlations involving a second harmonic are largest with $C_{2,2,4}$ being approximately 5 times larger in magnitude than the next largest correlator $C_{2,3,5}$. The correlations decrease quickly as harmonics are increased beyond $n=2$. The higher harmonic correlations $C_{3,3,6}$ and $C_{3,4,7}$ are both small but non-zero. The correlations $C_{1,1,2}, C_{1,2,3}, C_{2,2,4}, C_{2,3,5},$ and $C_{3,3,6}$ scaled by N_{part}^2 all exhibit extrema in mid central collisions where the initial overlap geometry is predominantly elliptical. We note that the centrality at which $N_{\text{part}}^2 C_{2,2,4}$ reaches a maximum is different than the centrality at which $N_{\text{part}}^2 C_{2,3,5}$ reaches a maximum.

As the collision energy is reduced, although the magnitude of the correlations becomes smaller, the centrality dependence and ordering of the different harmonics seems to remain mostly the same. The $C_{1,2,3}$ correlation

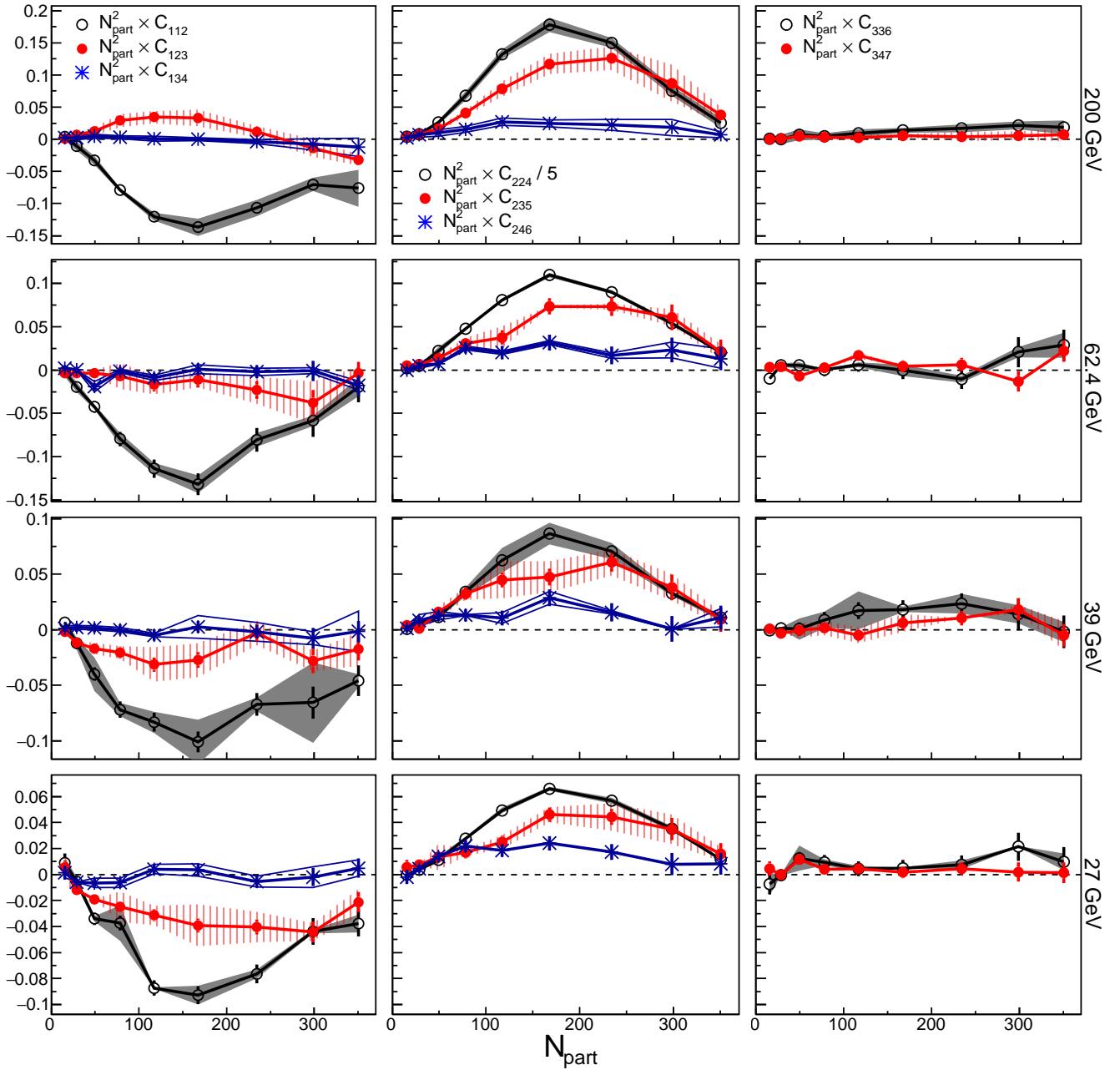


FIG. 5. (color online) The centrality dependence of the $C_{m,n,m+n}$ correlations scaled by N_{part}^2 for charged hadrons with $p_T > 0.2$ GeV/c and $|\eta| < 1$ from 200, 62.4, 39, and 27 GeV Au+Au collisions for $(m,n) = (1,1), (1,2), (1,3)$ (left) $(2,2), (2,3), (2,4)$ (center) and $(3,3), (3,4)$ (right). Systematic errors are shown as bands. All panels in the same row share the same scale but $C_{2,2,4}$ has been divided by a factor of 5 to fit on the panel. The labels in the top panels apply to all the panels in same column.

however is an exception. While at 200 GeV, $C_{1,2,3}$ is mostly positive, at 62.4 GeV it is consistent with zero or slightly negative and at lower energies it becomes more and more negative. We speculate that this behavior may be related to the increasing importance of momentum conservation as the number of particles produced in the collision decreases. No theoretical guidance exists however for the energy dependence of these correlations at

energies below 200 GeV. This data should provide useful constraints for the models being developed to describe lower energy collisions associated with the energy scan program at RHIC.

Figure 6 shows the same correlations as Fig. 5 except for lower energy data sets: $\sqrt{s_{\text{NN}}} = 19.6, 14.5, 11.5,$ and 7.7 GeV. Trends similar to those seen in Fig. 5 are for the most part also exhibited in this figure. Although the

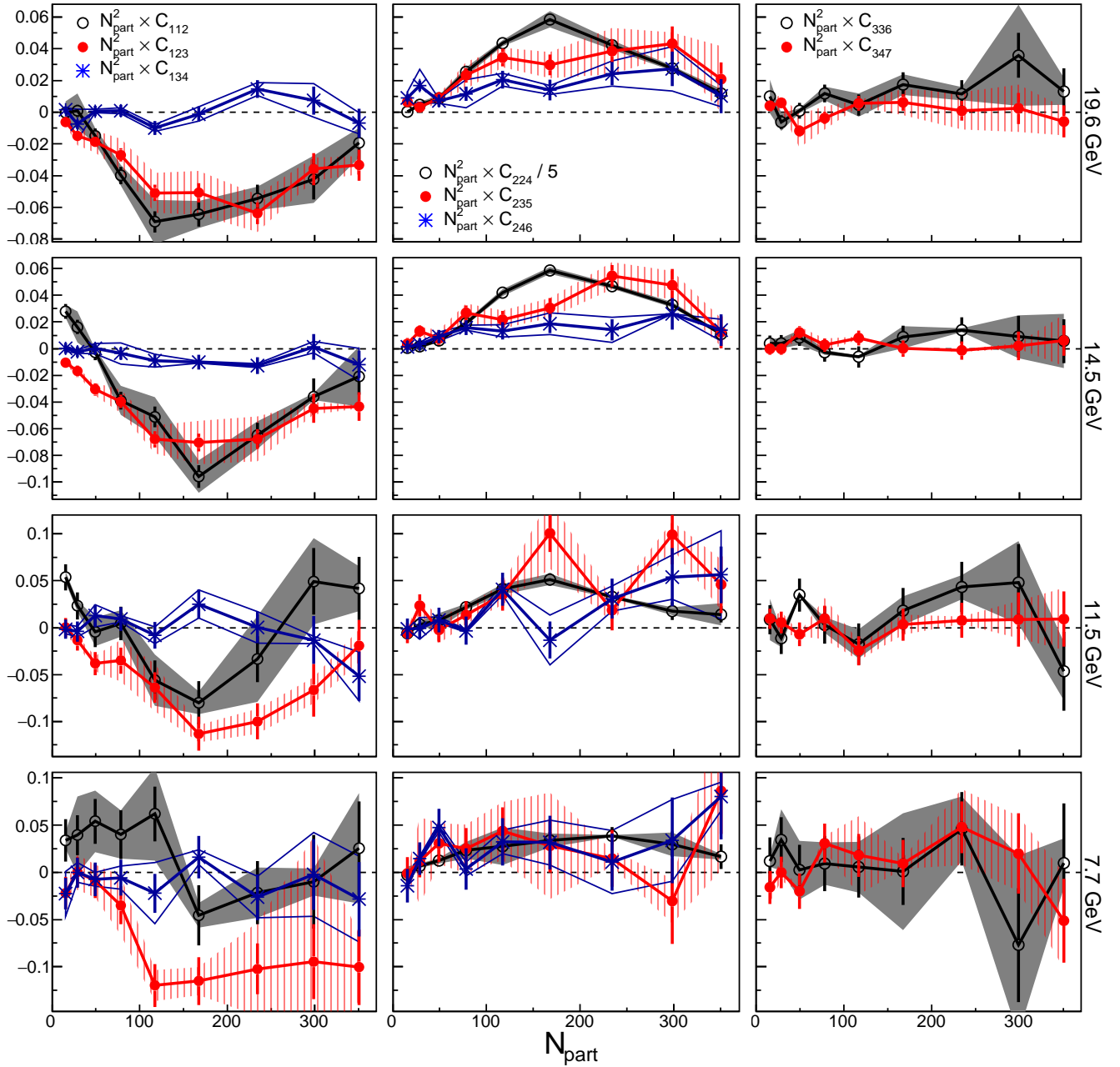


FIG. 6. (color online) The same quantities as Fig. 5 but for the lower energy Au+Au collisions 19.6, 14.5, 11.5, and 7.7 GeV.

statistical precision is poor for the lowest energy points, it appears that $C_{1,1,2}$ at 7.7 GeV is smaller in magnitude than at higher energies, becoming consistent with zero. This was also observed in the charge dependent measurements of $C_{1,1,2}$ [41]. A second phase of the RHIC beam energy scan planned for 2019 and 2020 will significantly increase the number of events available for analysis at these lower energies while expanding the η acceptance from $|\eta| < 1$ to $|\eta| < 1.5$ [42] so that this intriguing observation can be further investigated. The increased acceptance will increase the number of three-particle combina-

tions by approximately a factor of three and will make it possible to measure the $\Delta\eta$ dependence of the $C_{m,n,m+n}$ correlations to $|\Delta\eta| \approx 3$.

C. p_T Dependence

If the three-particle correlations presented here are dominated by correlations between event planes, then one might expect that the p_T dependence of the three-particle correlations will simply track the p_T dependence

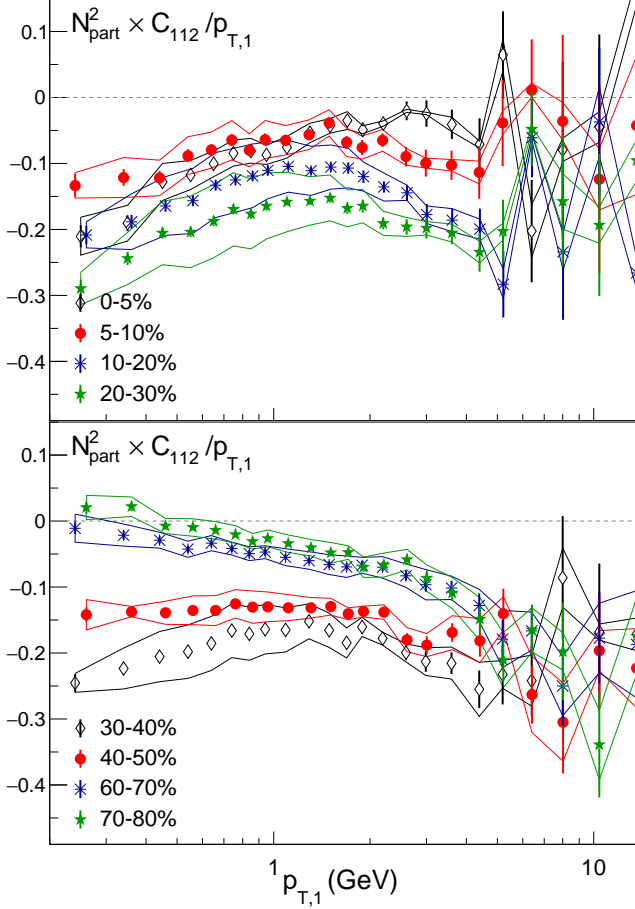


FIG. 7. (color online) Three-particle azimuthal correlations $C_{1,1,2}$ scaled by $N_{\text{part}}^2/p_{T,1}$ as a function of the first particles p_T for 200 GeV Au+Au collisions for charged hadrons with $p_T > 0.2$ GeV/c and $|\eta| < 1$. The top and bottom panels show the same quantity but for a different set of centrality intervals. Systematic errors are shown as solid lines enclosing the respective data points.

of the relevant v_n [22]:

$$\langle \cos(m\phi_1(p_T) + n\phi_2 - (m+n)\phi_3) \rangle \approx \frac{v_m(p_T)}{\varepsilon_m} \frac{v_n}{\varepsilon_n} \frac{v_{m+n}}{\varepsilon_{m+n}} \times \langle \varepsilon_m \varepsilon_n \varepsilon_{m+n} \cos(m\Psi_m + n\Psi_n - (m+n)\Psi_{m+n}) \rangle, \quad (2)$$

where ε_m is the m^{th} harmonic eccentricity and Ψ_m is the m^{th} harmonic participant plane angle. For the purpose of simplicity in this publication, we have scaled the correlations by N_{part}^2/p_T to account for the general increase of $v_n(p_T)$ with p_T [43]. That simple scaling is only valid at lower p_T and for $n \neq 1$. It does, however, aid in visualizing trends in the data which would otherwise be visually dominated by the larger p_T range. Our primary reason for introducing Eq. 2 is to provide a context for understanding the p_T dependence of $C_{m,n,m+n}$. The

relationship between $C_{m,n,m+n}$ and harmonic planes in Eq. 2 is not guaranteed to hold and is particularly likely to be broken for correlations involving the first harmonic where momentum conservation effects will likely play an important role or where a strong charge sign dependence has been observed [27, 28].

In Fig. 7 we show $N_{\text{part}}^2 C_{1,1,2}/p_T$ as a function of the p_T of particle one. The top panel shows the more central collisions while the bottom panel shows more peripheral collisions. In this and in the following figures related to the p_T dependence, we sometimes exclude centrality bins and slightly shift the positions of the points along the p_T axis to make the figures more readable. For more central collisions, $C_{1,1,2}/p_{T,1}$ is negative and slowly decreases in magnitude as $p_{T,1}$ increases. This indicates that $C_{1,1,2}$ is generally increasing with the p_T of particle one but that for central collisions at high p_T , $C_{1,1,2}$ starts to saturate. For the more peripheral 30-40% and 40-50% collision however, $C_{1,1,2}$ appears to be linear in p_T without an indication of saturation even up to $p_T \approx 10$ GeV/c. For the much more peripheral 60-70% and 70-80% centrality intervals, $C_{1,1,2}$ starts out at or above zero then becomes more and more negative as p_T is increased. The trends in the most peripheral centrality intervals, particularly at high p_T , are consistent with being dominated by momentum conservation and jets. A pair of back-to-back particles aligned with the reaction plane will lead to a negative value for $C_{1,1,2}$. Although the data exhibit a smooth transition from the trends in more central collisions to the trends in more peripheral collisions, the trends are quite distinct and indicative of very different correlations in those different regions. In peripheral collisions, the correlations get stronger as p_T is increased. In central collisions, the opposite is observed.

For the case of $C_{1,2,3}$ in Fig. 8, we show the p_T dependence of both particle one (left panels) and particle two (right panels). The dependence of $C_{1,2,3}/p_{T,2}$ on $p_{T,2}$ is quite weak indicating that where $C_{1,2,3}$ is non-zero, it increases roughly linearly with $p_{T,2}$. The dependence of $C_{1,2,3}/p_{T,1}$ on $p_{T,1}$, however, exhibits several notable trends. First we note that for the 20-30% centrality interval, $C_{1,2,3}/p_{T,1}$ changes sign up to three times. In hydrodynamic models, the value of $C_{1,2,3}$ is very sensitive to the interplay between linear and non-linear effects and to viscous effects. The sign oscillations exhibited in the data may be a consequence of subtle changes in the relevant sizes of those effects. If this is the case, then this confirms that $C_{1,2,3}$ is a powerful measurement to help tune those models. At intermediate $p_{T,1}$ (2-5 GeV/c), $C_{1,2,3}$ is positive for central collisions but negative for peripheral collisions. At $p_T > 7$ GeV/c, $C_{1,2,3}$ is strongly negative, perhaps again, indicative of the contribution of back-to-back jets to the correlations. Such strong negative correlation seems to be absent in central collisions where $C_{1,2,3}$ appears to remain positive, although with large error bars. This is consistent with a scenario where di-jets have been quenched in central collisions. As with $C_{1,1,2}$, the p_T trends for $C_{1,2,3}$ are very different in the

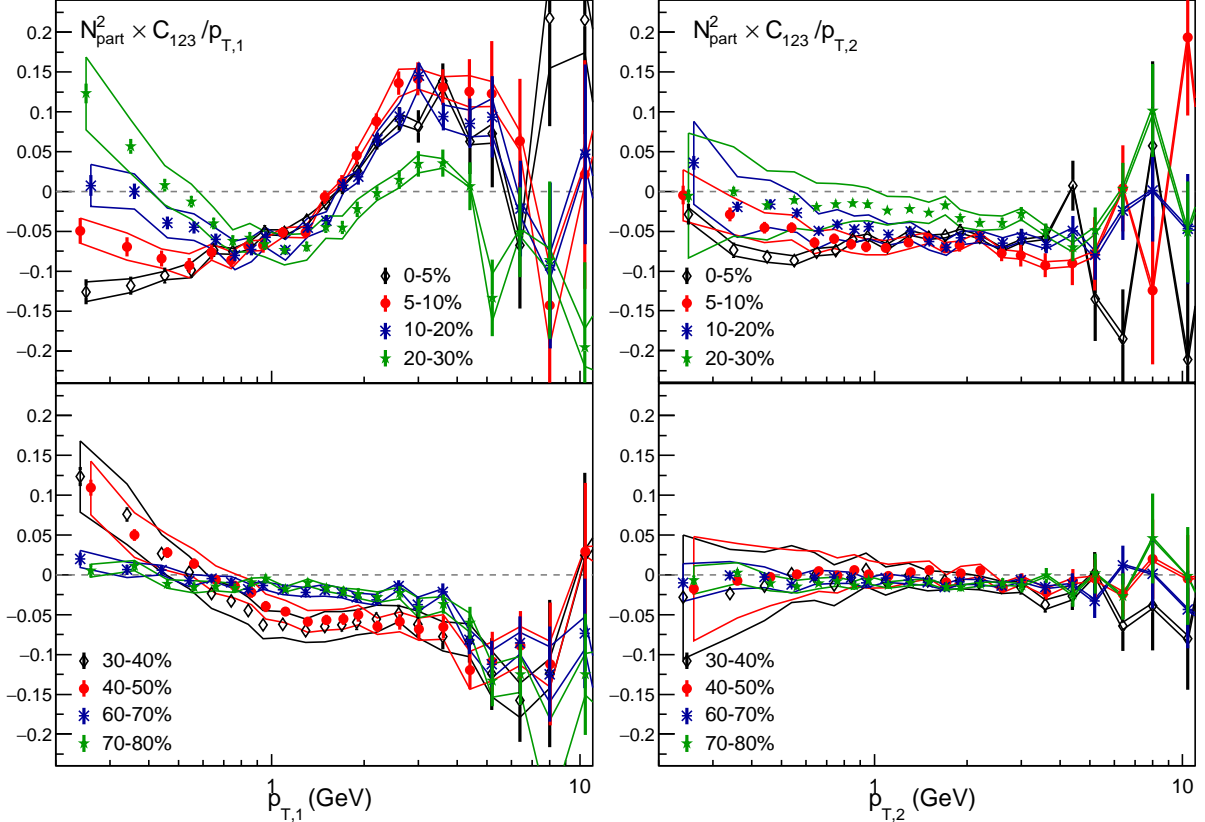


FIG. 8. (color online) Three-particle azimuthal correlations $C_{1,2,3}$ scaled by N_{part}^2/p_T as a function of the p_T using the p_T of particle one (left panels) or of particle two (right panels) for 200 GeV Au+Au collisions. Data are for charged hadrons with $p_T > 0.2$ GeV/c and $|\eta| < 1$. The top and bottom panels show the same quantity but for a different set of centrality intervals. Systematic errors are shown as solid lines enclosing the respective data points.

most peripheral and most central collisions.

The $C_{2,2,4}$ correlation is the largest of the $C_{m,n,m+n}$ correlations since it is strongly affected by the tendency of particles to preferentially line up with the reaction plane. In Fig. 9 we show $N_{\text{part}}^2 C_{2,2,4}/p_{T,1}$ as a function of $p_{T,1}$. At low $p_{T,1}$, the centrality dependence of the correlations is as expected from Fig. 5 (top panels) where we saw that the integrated value of $N_{\text{part}}^2 C_{2,2,4}$ is largest for mid-central collisions. This is a natural consequence of the fact that the initial second harmonic eccentricity decreases as collisions become more central while the efficiency of converting that eccentricity into momentum-space correlations increases (with multiplicity). The competition of these two trends leads to a maximum for second harmonic correlations in mid-central collisions. This well-known [43] and generic trend does not persist to higher values of $p_{T,1}$. We see a clear change in trends at $p_{T,1} > 5$ GeV/c with the most peripheral collisions having the largest correlation strength while $N_{\text{part}}^2 C_{2,2,4}/p_{T,1}$ drops significantly as a function of $p_{T,1}$ for the mid-central collisions. We note that past measurements of p_T spectra and $v_2(p_T)$ for identified particles have indicated that the effects of flow may persist

up to 5 or 6 GeV/c [43]. This observation is consistent with model calculations that show in a parton cascade even up to $p_T \approx 5$ GeV/c there are a significant number of partons whose final momentum has been increased by interactions with the medium [44]. The $p_{T,1}$ dependence of $C_{2,2,4}/p_{T,1}$ supports that picture as well.

In Fig. 10, we show the p_T dependence of $N_{\text{part}}^2 C_{2,3,5}/p_T$ where p_T is either the p_T of particle one (left panels) or particle two (right panels). Again, the top panels show more central collisions and the bottom panels more peripheral. For $p_T < 5$, $C_{2,3,5}/p_T$ is mostly flat as a function of the p_T of either particle one or particle two. Above that, the correlations seem to become smaller but with large statistical errors. One can discern a slight difference between the trends in the left and right panels: $C_{2,3,5}/p_{T,1}$ seems to decrease slightly as a function of $p_{T,1}$, while $C_{2,3,5}/p_{T,2}$ as a function of $p_{T,2}$ seems to increase slightly. This is likely related to the different p_T dependences of v_2 and v_3 where v_2 has been found to saturate at lower p_T while v_3 is still growing. In central collisions, it is even found that v_3 becomes larger than v_2 at intermediate p_T [16].

We have tried to point out interesting features in the

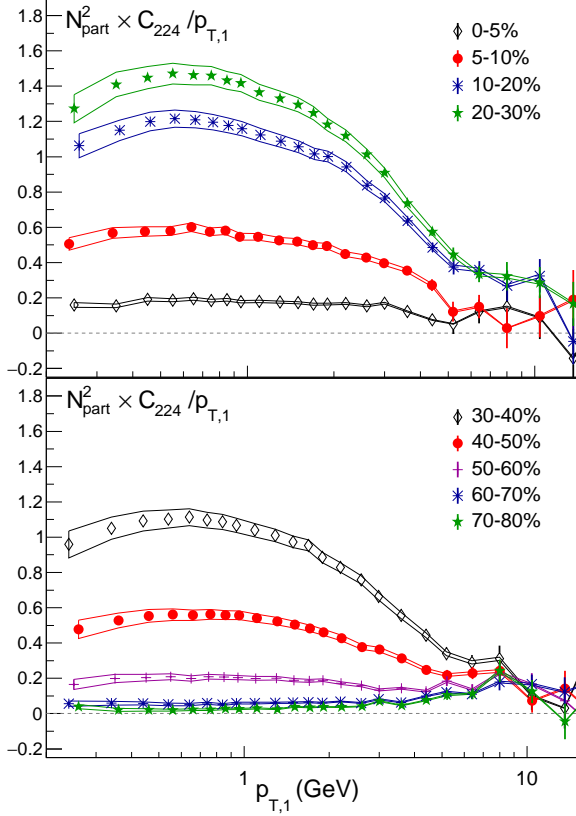


FIG. 9. (color online) Three-particle azimuthal correlations $C_{2,2,4}$ scaled by $N_{\text{part}}^2/p_{T,1}$ as a function of $p_{T,1}$ for 200 GeV Au+Au collisions. Data are for charged hadrons with $p_T > 0.2$ GeV/c and $|\eta| < 1$. The top and bottom panels show the same quantity but for a different set of centrality intervals. Systematic errors are shown as solid lines enclosing the respective data points.

p_T dependence of the correlations. In particular, we note that the p_T trends are very different when comparing central collisions to peripheral collisions. We expect that when these data are compared to model calculations, they will provide even greater insights into the interplay between the effects of hard scattering, shear viscosity, bulk viscosity, the collision life-time and non-linear couplings between harmonics.

D. Energy Dependence

While Figs. 5 and 6 show the centrality dependence of 8 different $C_{m,n,m+n}$ correlations for 8 beam energies, in this section we will investigate the energy dependence in greater detail by first showing the centrality dependence of individual $C_{m,n,m+n}$ correlations for a variety of energies in single panels for easier comparison. We will then show correlations at specific centrality intervals as a function of $\sqrt{s_{\text{NN}}}$ scaled by v_2 . Finally we will discuss

implications of the energy dependence of the correlations.

Figure 11 shows the centrality dependence of $N_{\text{part}}^2 C_{1,1,2}$ (left) and $N_{\text{part}}^2 C_{1,2,3}$ (right) for 200, 62.4, 27, 14.5, and 7.7 or 11.5 GeV collisions. Some energies are omitted for clarity. For $N_{\text{part}}^2 C_{1,1,2}$, the general centrality trend appears to remain the same at all energies except 7.7 GeV, even though the magnitude slightly decreases. For mid-central collisions, $C_{1,1,2}$ is negative for all the energies shown. The 7.7 GeV data may deviate from the trend observed for the other energies as will be discussed later. For $N_{\text{part}}^2 C_{1,2,3}$, the energy dependence is quite different. The only positive values for $C_{1,2,3}$ are for 200 GeV collisions. At 62.4 GeV, $N_{\text{part}}^2 C_{1,2,3}$ has a slightly negative value that is within errors, independent of centrality. As the energy decreases, $C_{1,2,3}$ becomes more negative so that the centrality dependence of $C_{1,2,3}$ at 14.5 GeV is nearly the mirror reflection of the 200 GeV data. As will be discussed below, the change in sign of $C_{1,2,3}$ has interesting implications for how two-particle correlations relative to the reaction plane change as a function of beam energy.

Figure 12 shows the centrality dependence of $N_{\text{part}}^2 C_{2,2,4}$ and $N_{\text{part}}^2 C_{2,3,5}$ for a selection of collision energies. Both $C_{2,2,4}$ and $C_{2,3,5}$ remain positive for the centralities and energies shown with no apparent changes in the centrality trends. We note that although $C_{2,2,4}$ drops significantly from 200 down to 19.6 GeV, we observe little change with energy below 19.6 GeV. A similar lack of energy dependence between 7.7 and 19.6 GeV was also observed in recent measurements of $v_3^2\{2\}$ [18]. This is notable since one would naively expect either of these correlation measurements to continuously increase as the density of the collision region increases.

To better view the energy trends, in Fig. 13 we show $N_{\text{part}} C_{m,n,m+n}/v_2$ as a function of $\sqrt{s_{\text{NN}}}$ for three centrality intervals: 10-20%, 20-30%, and 30-40%. The v_2 values are based on a two-particle cumulant analysis as discussed in Appendix A. The scaling will be further discussed in the next paragraph. For all centrality intervals shown, $C_{1,1,2}/v_2$ is negative at the highest energy but the magnitude of the correlation decreases as the energy decreases and becomes consistent with zero, although with large errors, at 7.7 GeV. This behavior was also observed in the charge dependence of this correlator which has been studied to search for the charge separation predicted to be a consequence of the chiral magnetic effect [41]. As noted above, both $C_{2,2,4}$ and $C_{2,3,5}$ are positive for all energies. The energy dependence of $C_{1,2,3}/v_2$ is unique in that it is positive at 200 GeV but then drops below zero near 62.4 GeV and continues to become more negative at lower energies. In the following paragraph, we discuss the implications that this trend has for how two-particle correlations with respect to the reaction plane change with energy.

The correlations $C_{1,1,2}$, $C_{1,2,3}$, $C_{2,2,4}$, and $C_{2,3,5}$ presented in Fig. 13 have either $m = 2$, $n = 2$, or $m+n = 2$. When v_2 is large, as it is for the 10-20%, 20-30% and 30-40% centrality intervals, then $\langle \cos(1\phi_1 + 1\phi_2 - 2\phi_3) \rangle / v_2 \approx$

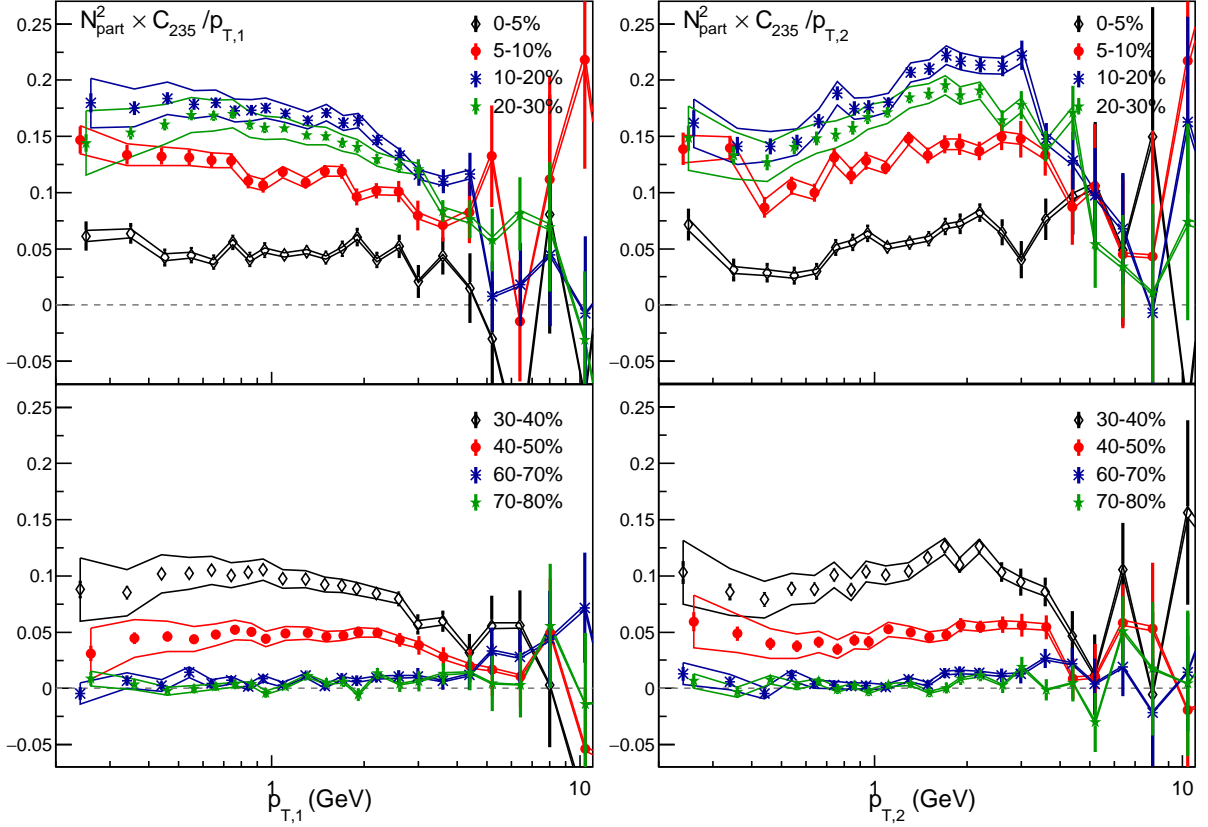


FIG. 10. (color online) Three-particle azimuthal correlations $C_{2,3,5}$ scaled by N_{part}^2/p_T as a function of p_T where the p_T is taken for either particle one (left panels) or particle two (right panels) for 200 GeV Au+Au collisions. Data are for charged hadrons with $p_T > 0.2$ GeV/c and $|\eta| < 1$. The top and bottom panels show the same quantity but for a different set of centrality intervals. Systematic errors are shown as solid lines enclosing the respective data points.

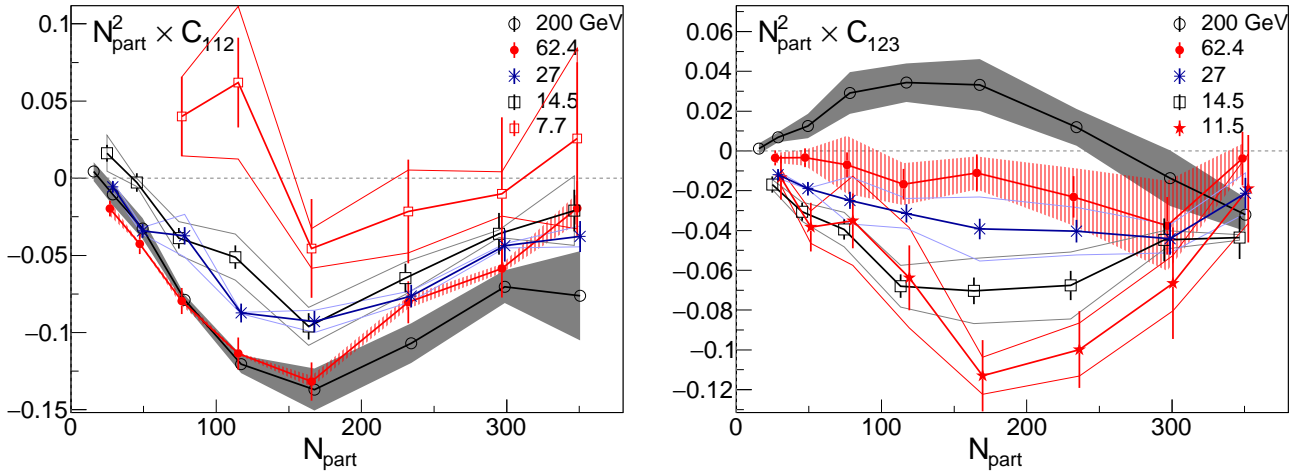


FIG. 11. (color online) The centrality dependence of $C_{1,1,2}$ (left) and $C_{1,2,3}$ (right) scaled by N_{part}^2 for a selection of energies.

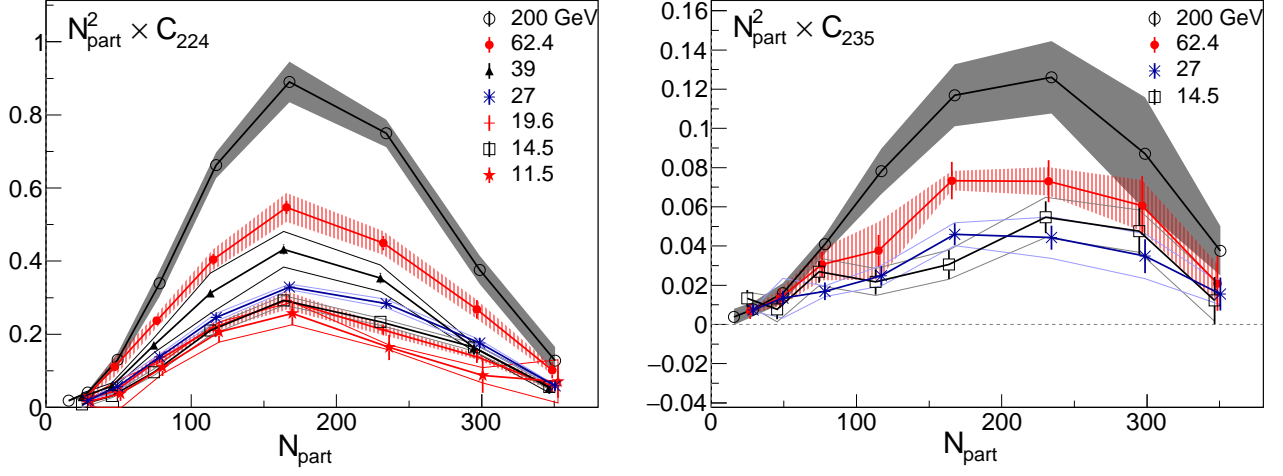


FIG. 12. (color online) The centrality dependence of $C_{2,2,4}$ (left) and $C_{2,3,5}$ (right) scaled by N_{part}^2 for a selection of energies.

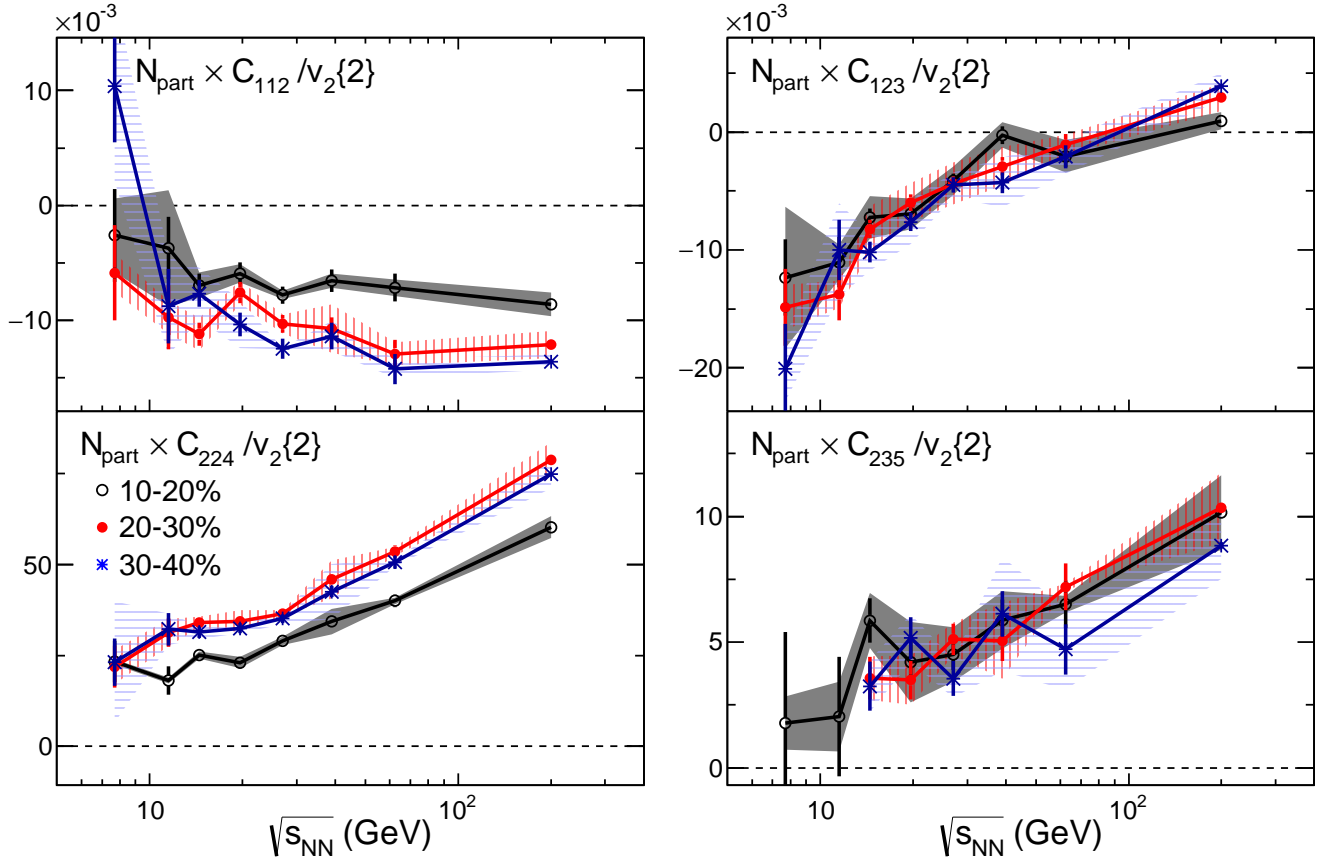


FIG. 13. (color online) The $\sqrt{s_{\text{NN}}}$ dependence of $N_{\text{part}} C_{m,n,m+n} / v_2$ for $(m,n) = (1,1)$ (top left), $(1,2)$ (top right), $(2,2)$ (bottom left) and $(2,3)$ (bottom right) for three selected centrality intervals. In the bottom right panel, the lowest energy points for the 20-30% and 30-40% centrality intervals, having large uncertainties, are omitted for clarity. Statistical uncertainties are shown as vertical error bars while the systematic errors are shown as shaded regions or bands.

$\langle \cos(1\phi_1 + 1\phi_2 - 2\Psi_{\text{RP}}) \rangle$ and $\langle \cos(2\phi_1 + m\phi_2 - (m+2)\phi_3) \rangle / v_2 \approx \langle \cos(2\Psi_{\text{RP}} + m\phi_2 - (m+2)\phi_3) \rangle$ where Ψ_{RP} is the reaction plane angle. Correlations including a second harmonic should then provide information about two-particle correlations with respect to the second harmonic reaction plane:

$$\begin{aligned} \langle \cos(1\phi_1 + 1\phi_3 - 2\phi_2) \rangle / v_2 &\approx \langle \cos(1\phi'_1 + 1\phi'_2) \rangle, \\ \langle \cos(1\phi_1 + 2\phi_3 - 3\phi_2) \rangle / v_2 &\approx \langle \cos(1\phi'_1 - 3\phi'_2) \rangle, \\ \langle \cos(2\phi_1 + 2\phi_3 - 4\phi_2) \rangle / v_2 &\approx \langle \cos(2\phi'_1 - 4\phi'_2) \rangle, \\ \langle \cos(2\phi_3 + 3\phi_1 - 5\phi_2) \rangle / v_2 &\approx \langle \cos(3\phi'_1 - 5\phi'_2) \rangle, \end{aligned} \quad (3)$$

where $\phi' = \phi - \Psi_{\text{RP}}$. Since we are integrating over all particles in these correlations, the subscript label for the particles is arbitrary so we have reassigned them so that particle 3 is always associated with the second harmonic. For illustration, Table I shows values for $C_{m,n,m+n}/v_2$ for specific values of ϕ'_1 and ϕ'_2 . At 200 GeV, all measured correlations are positive except $\langle \cos(\phi'_1 + \phi'_2) \rangle$. This points to an enhanced probability for a pair of particles in one of two possible configurations: either $\phi'_1 \approx \pi/3$ and $\phi'_2 \approx 2\pi/3$ or $\phi'_1 \approx -\pi/3$ and $\phi'_2 \approx -2\pi/3$ (these correspond to the right-most column of Table I). This result is surprising since it implies a preference for both of the correlated particles to either be in the upper hemisphere, or both in the lower hemisphere. We note however, that hydrodynamic models with fluctuating initial conditions correctly predict this trend [45] which could arise from increased density fluctuations at either the top or the bottom of the almond shaped overlap region. A high density fluctuation in the lower half of the almond zone naturally leads to particles moving upward and away from that density fluctuation so that they both end up in the upper hemisphere. This response was described in Ref. [22] and was illustrated as ‘‘Position B’’ in Fig. IV of that reference. For energies below 200 GeV, $C_{1,2,3}$ changes sign so that $\langle \cos(\phi'_1 + \phi'_2) \rangle$ and $\langle \cos(1\phi'_1 - 3\phi'_2) \rangle$ are both negative while $\langle \cos(2\phi'_1 - 4\phi'_2) \rangle$ and $\langle \cos(3\phi'_1 - 5\phi'_2) \rangle$ are both positive. This condition does not match any of the scenarios in the table but it could indicate an increased preference for particle pairs with $\phi'_1 \approx 0$ and $\phi'_2 \approx \pi$. A preference for back-to-back particle pairs aligned with the reaction plane would be consistent with an increased importance for momentum conservation at lower energies. Momentum conservation naturally leads to a tendency for particles to be emitted with back-to-back azimuth angles [46]. As the beam energy is decreased, the multiplicity decreases and we should expect the effects of momentum conservation to become more prominent (in the case that only two particles are emitted, they must be back-to-back). The implications of this change in the configuration of two-particle correlations with respect to the reaction plane deserves further theoretical investigation.

The discussion in the above paragraph illustrates how measurements of $C_{m,n,m+n}$ reveal information about two-particle correlations with respect to the reaction plane and we pointed out two specific conclusions based

TABLE I. Values for $C_{m,n,m+n}/v_2$ for specific cases of ϕ'_1 and ϕ'_2 where $\phi' = \phi - \Psi_{\text{RP}}$ (see Eq. 3). The first column ($\phi'_1 = \phi'_2 = 0$) corresponds to a particle pair with $\Delta\phi = 0$ emitted in the direction of the reaction plane (in-plane). The second column corresponds to back-to-back ($\Delta\phi = \pi$) particles emitted in-plane. The third and fourth columns correspond to pairs of particles emitted perpendicular to the reaction plane (out-of-plane) with either $\Delta\phi = 0$ or $\Delta\phi = \pi$ respectively. The right-most column is a scenario consistent with the correlations observed in mid-central collisions at $\sqrt{s_{\text{NN}}} = 200$ GeV.

	(ϕ'_1, ϕ'_2) [rad]				
	$(0, 0)$	$(0, \pi)$	$\pm(\frac{\pi}{2}, \frac{\pi}{2})$	$(\frac{\pi}{2}, -\frac{\pi}{2})$	$\pm(\frac{\pi}{3}, \frac{2\pi}{3})$
$C_{1,1,2}/v_2$	+1	-1	-1	+1	-1
$C_{1,2,3}/v_2$	+1	-1	-1	+1	$+\frac{1}{2}$
$C_{2,2,4}/v_2$	+1	+1	-1	-1	+1
$C_{2,3,5}/v_2$	+1	-1	-1	+1	$+\frac{1}{2}$

on the p_T - and $\Delta\eta$ -integrated measurements. The value of $C_{1,2,3}$ changes sign as a function of centrality, $\Delta\eta$ and p_T suggesting that further specific configurations may arise when triggering on a particular p_T or investigating particles separated by an η -gap. We have not examined the charge dependence of $C_{m,n,m+n}$ but future work placing a like-sign or unlike-sign requirement on ϕ'_1 and ϕ'_2 may be useful for interpreting charge separation measurements and determining whether they should be taken as evidence for the chiral magnetic effect.

IV. CONCLUSIONS

We presented measurements of the energy, centrality, p_T , and $\Delta\eta$ dependence of three-particle azimuthal correlations $C_{m,n,m+n}$ for a variety of combinations of m and n . We find a strong dependence of $C_{1,1,2}$ on $|\eta_1 - \eta_2|$ and a strong dependence of $C_{1,2,3}$ on $|\eta_1 - \eta_3|$. Meanwhile, $C_{2,2,4}$ and $C_{2,3,5}$ exhibit a smaller but still appreciable dependence on $|\eta_1 - \eta_3|$. This may indicate either the presence of short-range non-flow correlations or a rapidity dependence to the initial energy density signaling a breaking of longitudinal invariance. Simple pictures of non-flow however, appear to be inconsistent with the overall trends observed in the data. The integrated correlations with $m = 1$ are generally negative or consistent with zero except for $C_{1,2,3}$ which, at 200 GeV, is positive for mid-central collisions while it is negative for all centralities at all of the lower energies. Nonzero values for $C_{1,2,3}$ imply correlations between the second and third harmonic event plane that are predicted from models of the initial overlap geometry. The p_T dependence of the correlations exhibits trends suggesting significant differences between the correlations in peripheral colli-

sions and more central collisions as well as differences for $p_T > 5$ GeV/c and $p_T < 5$ GeV/c. The quantity $C_{1,2,3}$ as a function of $p_{T,1}$ changes sign as many as three times. While $C_{1,1,2}$ is negative for higher energies, it becomes positive or consistent with zero at 7.7 GeV. By examining the energy dependence of $C_{1,1,2}$, $C_{1,2,3}$, $C_{2,2,4}$, and $C_{2,3,5}$ divided by v_2 we are able to infer that in mid-central collisions at 200 GeV, there is a preference for particle pairs to be emitted with angles relative to the reaction plane of either $\phi_1 \approx \pi/3$ and $\phi_2 \approx 2\pi/3$ or $\phi_1 \approx -\pi/3$ and $\phi_2 \approx -2\pi/3$. At 62.4 GeV and below, this appears to change due to a possible preference for back-to-back pairs ($\phi_1 \approx 0$ and $\phi_2 \approx \pi$) aligned with the reaction plane. These data will be useful for constraining hydrodynamic models. Measurements of the charge dependence of the correlations presented here, by revealing information about the preferred directions of correlated particles with respect to the reaction plane, should provide valuable insights into whether or not the charge separation observed in heavy-ion collisions is related to the chiral magnetic effect.

ACKNOWLEDGMENTS

We thank the RHIC Operations Group and RCF at BNL, the NERSC Center at LBNL, and the Open Science Grid consortium for providing resources and support. This work was supported in part by the Office of Nuclear Physics within the U.S. DOE Office of Science, the U.S. National Science Foundation, the Ministry of Education and Science of the Russian Federation, National Natural Science Foundation of China, Chinese Academy of Science, the Ministry of Science and Technology of China and the Chinese Ministry of Education, the National Research Foundation of Korea, GA and MSMT of the Czech Republic, Department of Atomic Energy and Department of Science and Technology of the Government of India; the National Science Centre of Poland, National Research Foundation, the Ministry of Science, Education and Sports of the Republic of Croatia, RosAtom of Russia and German Bundesministerium für Bildung, Wissenschaft, Forschung und Technologie (BMBF) and the Helmholtz Association.

Appendix A: Two-particle Cumulants $v_n^2\{2\}$

In this appendix we present the measurements of $v_n^2\{2\}$ for $n=1, 2, 4$ and 5. The second harmonic $v_2^2\{2\}$ was used

to scale $C_{m,n,m+n}$ in Fig. 13. Under the assumption that

$$\langle \cos(m\phi_1 + n\phi_2 - (m+n)\phi_3) \rangle \approx \langle v_m v_n v_{m+n} \cos(m\Psi_m + n\Psi_n - (m+n)\Psi_{m+n}) \rangle \quad (\text{A1})$$

where Ψ_m is the participant plane angle for harmonic m , one can convert the $C_{m,n,m+n}$ correlations into reaction plane correlations in the low-resolution limit by dividing by $\sqrt{v_m^2\{2\}v_n^2\{2\}v_{m+n}^2\{2\}}$. The relationship of the $C_{m,n,m+n}$ to v_m and Ψ_m assumes that non-flow correlations are minimal. Similar assumptions must also be made when using event-plane angles in the analysis. The analysis of $v_n^2\{2\}$ was performed in a similar manner to that of $v_3^2\{2\}$ presented in Ref. [18]. The $\Delta\eta$ dependence of $\langle \cos 2(\phi_1 - \phi_2) \rangle$ is analyzed for $p_T > 0.2$ GeV/c and $|\eta| < 1$. Short-range correlations are parameterized with a narrow Gaussian peak centered at $\Delta\eta = 0$ and the remaining longer-range correlations are integrated (weighting by the number of pairs at each $\Delta\eta$) to obtain the $\Delta\eta$ -integrated $v_n^2\{2\}$ results. The quantity labeled v_2 in Fig. 13 is $\sqrt{v_2^2\{2\}}$.

Figure 14 shows the results for $v_1^2\{2\}$ (left) and $v_2^2\{2\}$ (right) as a function of centrality for 200, 62.4, 39, 27, 19.6, 14.5, 11.5, and 7.7 GeV Au+Au collisions. The data are scaled by N_{part} and plotted versus N_{part} for convenience. At 200 GeV, $v_1^2\{2\}$ is positive for central collisions but becomes negative for $N_{\text{part}} < 150$. The negative values are expected from momentum conservation and present a conceptual challenge for dividing $C_{m,n,m+n}$ by $\sqrt{v_n^2\{2\}}$. The values of $v_1^2\{2\}$ become more negative at lower energies. This is consistent again with momentum conservation effects which are expected to become stronger as multiplicity decreases. In the limit of a collision that produces only two particles, momentum conservation would require that $v_1^2\{2\} = -1$. The $v_1^2\{2\}$ results follow a monotonic energy trend except for peripheral collisions at 19.6 GeV which appear to be elevated with respect to the trends.

The right panel of Fig. 14 shows the results for $N_{\text{part}}v_2^2\{2\}$ which remain positive for all energies and collision centralities. While it is unusual to scale $v_2^2\{2\}$ by N_{part} , we keep this format for consistency. The scaled results exhibit a strong peak for mid-central collisions due to the elliptic geometry of those collisions.

Figure 15 shows the data for $N_{\text{part}}v_4^2\{2\}$ (left) and $N_{\text{part}}v_5^2\{2\}$ (right) for a more limited energy range. Results for $N_{\text{part}}v_3^2\{2\}$ are available in Ref. [18]. At the lower energies the relative uncertainties on these data become too large to be of use. This presents another challenge to recasting $C_{m,n,m+n}$ in terms of reaction plane correlations because scaling by $\sqrt{v_4^2\{2\}}$ or $\sqrt{v_5^2\{2\}}$ leads to a large uncertainty on the resulting ratios.

[1] J. C. Collins and M. J. Perry, ‘‘Superdense Matter: Neutrons Or Asymptotically Free Quarks?,’’ Phys. Rev. Lett.

34, 1353 (1975).

[2] S. A. Chin, ‘‘Transition to Hot Quark Matter in Relativis-

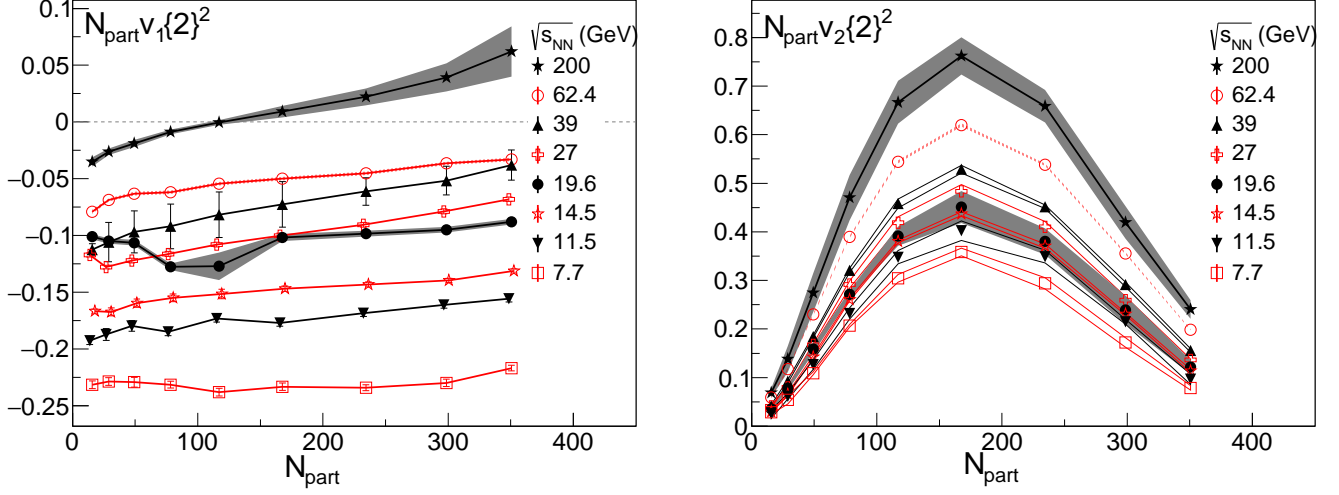


FIG. 14. The $\sqrt{s_{NN}}$ dependence and centrality dependence of $N_{\text{part}}v_1^2\{2\}$ (left) and $N_{\text{part}}v_2^2\{2\}$ (right) after short-range correlations, predominantly from quantum and Coulomb effects, have been subtracted. For more details see Ref. [18]. The centrality intervals correspond to 0-5%, 5-10%, 10-20%, 20-30%, 30-40%, 40-50%, 50-60%, 60-70% and 70-80%. The N_{part} values used for the corresponding centralities are 350.6, 298.6, 234.3, 167.6, 117.1, 78.3, 49.3, 28.2 and 15.7 independent of energy.

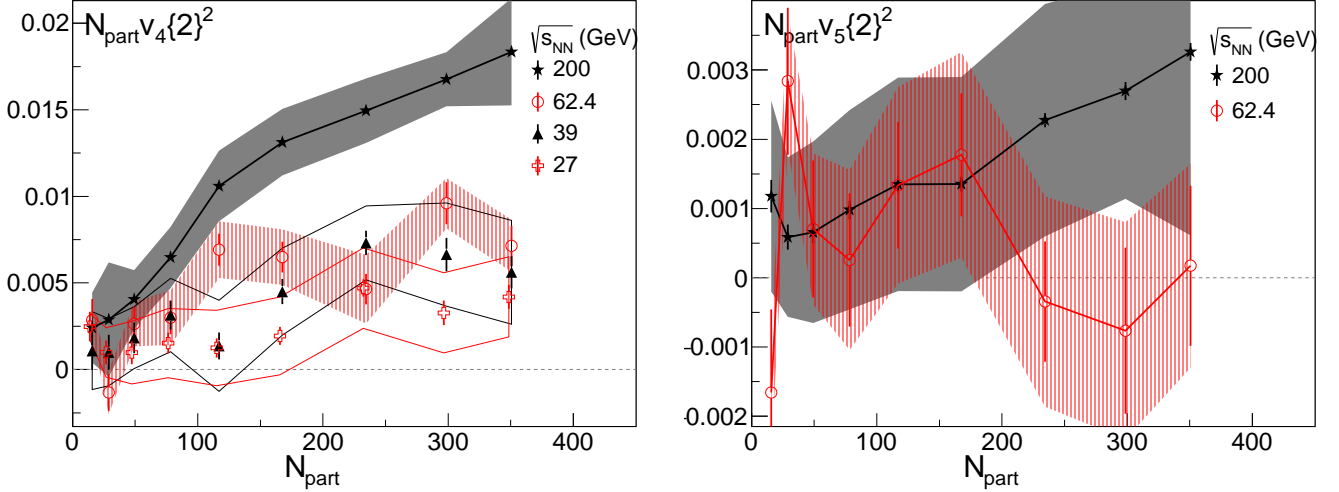


FIG. 15. The $\sqrt{s_{NN}}$ dependence and centrality dependence of $N_{\text{part}}v_4^2\{2\}$ (left) and $N_{\text{part}}v_5^2\{2\}$ (right) after short-range correlations, predominantly from Quantum and Coulomb effects, have been subtracted. For more details see Ref. [18].

tic Heavy Ion Collision,” Phys. Lett. B **78**, 552 (1978).
 [3] J. I. Kapusta, “Quantum Chromodynamics at High Temperature,” Nucl. Phys. B **148**, 461 (1979).
 [4] R. Anishetty, P. Koehler and L. D. McLerran, “Central Collisions Between Heavy Nuclei at Extremely High-Energies: The Fragmentation Region,” Phys. Rev. D **22**, 2793 (1980).
 [5] S. Borsanyi *et al.* [Wuppertal-Budapest Collaboration], “Is there still any T_c mystery in lattice QCD? Results with physical masses in the continuum limit III,” JHEP **1009**, 073 (2010).
 [6] T. Bhattacharya *et al.*, “QCD Phase Transition with Chiral Quarks and Physical Quark Masses,” Phys. Rev. Lett. **113**, 082001 (2014).

[7] Y. Aoki, G. Endrodi, Z. Fodor, S. D. Katz and K. K. Szabo, “The Order of the quantum chromodynamics transition predicted by the standard model of particle physics,” Nature **443**, 675 (2006).
 [8] M. M. Aggarwal *et al.* [STAR Collaboration], “An Experimental Exploration of the QCD Phase Diagram: The Search for the Critical Point and the Onset of Deconfinement,” arXiv:1007.2613 [nucl-ex].
 [9] S. A. Voloshin, A. M. Poskanzer, R. Snellings, “Collective phenomena in non-central nuclear collisions,” [arXiv:0809.2949 [nucl-ex]]; P. Sorensen, “Elliptic Flow: A Study of Space-Momentum Correlations In Rela-

- tivistic Nuclear Collisions,” [arXiv:0905.0174 [nucl-ex]]; H. G. Ritter and R. Stock, “Collective Flow of QCD Matter: a Historical Introduction,” *J. Phys. G* **41**, 124002 (2014).
- [10] J. Adams *et al.* [STAR Collaboration], “Minijet deformation and charge-independent angular correlations on momentum subspace (η , ϕ) in Au-Au collisions at $\sqrt{s_{NN}} = 130$ GeV,” *Phys. Rev. C* **73**, 064907 (2006); J. Adams *et al.* [STAR Collaboration], “Delta ϕ Delta η Correlations in Central Au+Au Collisions at $\sqrt{s_{NN}} = 200$ GeV,” *Phys. Rev. C* **75**, 034901 (2007); A. Adare *et al.* [PHENIX Collaboration], “Dihadron azimuthal correlations in Au+Au collisions at $\sqrt{s_{NN}} = 200$ GeV,” *Phys. Rev. C* **78** (2008) 014901; B. I. Abelev *et al.* [STAR Collaboration], “Long range rapidity correlations and jet production in high energy nuclear collisions,” *Phys. Rev. C* **80**, 064912 (2009); B. Alver *et al.* [PHOBOS Collaboration], “High transverse momentum triggered correlations over a large pseudorapidity acceptance in Au+Au collisions at $\sqrt{s_{NN}} = 200$ GeV,” *Phys. Rev. Lett.* **104**, 062301 (2010); S. Chatrchyan *et al.* [CMS Collaboration], “Long-range and short-range dihadron angular correlations in central PbPb collisions at a nucleon-nucleon center of mass energy of 2.76 TeV,” *JHEP* **1107**, 076 (2011); K. Aamodt *et al.* [ALICE Collaboration], “Harmonic decomposition of two-particle angular correlations in Pb-Pb collisions at $\sqrt{s_{NN}} = 2.76$ TeV,” *Phys. Lett. B* **708**, 249 (2012); G. Aad *et al.* [ATLAS Collaboration], “Measurement of the azimuthal anisotropy for charged particle production in $\sqrt{s_{NN}} = 2.76$ TeV lead-lead collisions with the ATLAS detector,” *Phys. Rev. C* **86**, 014907 (2012).
- [11] S. A. Voloshin, “Two particle rapidity, transverse momentum, and azimuthal correlations in relativistic nuclear collisions and transverse radial expansion,” *Nucl. Phys. A* **749**, 287 (2005).
- [12] A. P. Mishra, R. K. Mohapatra, P. S. Saumia, A. M. Srivastava, “Super-horizon fluctuations and acoustic oscillations in relativistic heavy-ion collisions,” *Phys. Rev. C* **77**, 064902 (2008).
- [13] P. Sorensen, “Searching for Superhorizon Fluctuations in Heavy-Ion Collisions,” [arXiv:0808.0503 [nucl-ex]]; P. Sorensen, “Implications of space-momentum correlations and geometric fluctuations in heavy-ion collisions,” *J. Phys. G* **37**, 094011 (2010).
- [14] J. Takahashi *et al.*, “Topology studies of hydrodynamics using two particle correlation analysis,” *Phys. Rev. Lett.* **103**, 242301 (2009).
- [15] P. Sorensen, B. Bolliet, A. Mocsy, Y. Pandit and N. Pruthi, “The Rise and Fall of the Ridge in Heavy Ion Collisions,” *Phys. Lett. B* **705**, 71 (2011).
- [16] K. Aamodt *et al.* [ALICE Collaboration], “Higher harmonic anisotropic flow measurements of charged particles in Pb-Pb collisions at $\sqrt{s_{NN}}=2.76$ TeV,” *Phys. Rev. Lett.* **107**, 032301 (2011), A. Adare *et al.* [PHENIX Collaboration], “Measurements of Higher-Order Flow Harmonics in Au+Au Collisions at $\sqrt{s_{NN}} = 200$ GeV,” *Phys. Rev. Lett.* **107**, 252301 (2011), L. Adamczyk *et al.* [STAR Collaboration], “Third Harmonic Flow of Charged Particles in Au+Au Collisions at $\sqrt{s_{NN}} = 200$ GeV,” *Phys. Rev. C* **88**, 014904 (2013).
- [17] C. Adler *et al.* [STAR Collaboration], “Elliptic flow from two and four particle correlations in Au+Au collisions $\sqrt{s_{NN}} = 130$ GeV,” *Phys. Rev. C* **66**, 034904 (2002).
- [18] L. Adamczyk *et al.* [STAR Collaboration], “Beam Energy Dependence of the Third Harmonic of Azimuthal Correlations in Au+Au Collisions at RHIC,” *Phys. Rev. Lett.* **116**, 112302 (2016).
- [19] R. S. Bhalerao, J. Y. Ollitrault and S. Pal, “Event-plane correlators,” *Phys. Rev. C* **88**, 024909 (2013).
- [20] J. D. Bjorken, “Highly Relativistic Nucleus-Nucleus Collisions: The Central Rapidity Region,” *Phys. Rev. D* **27**, 140 (1983).
- [21] G. Denicol, A. Monnai and B. Schenke, “Moving forward to constrain the shear viscosity of QCD matter,” *Phys. Rev. Lett.* **116**, 212301 (2016).
- [22] D. Teaney and L. Yan, “Triangularity and Dipole Asymmetry in Heavy Ion Collisions,” *Phys. Rev. C* **83**, 064904 (2011).
- [23] Z. Qiu and U. Heinz, “Hydrodynamic event-plane correlations in Pb+Pb collisions at $\sqrt{s} = 2.76$ ATeV,” *Phys. Lett. B* **717**, 261 (2012).
- [24] D. Teaney and L. Yan, “Event-plane correlations and hydrodynamic simulations of heavy ion collisions,” *Phys. Rev. C* **90**, 024902 (2014).
- [25] H. Niemi, K. J. Eskola and R. Paatelainen, “Event-by-event fluctuations in perturbative QCD + saturation + hydro model: pinning down QCD matter shear viscosity in ultrarelativistic heavy-ion collisions,” arXiv:1505.02677 [hep-ph].
- [26] S. Ryu, J.-F. Paquet, C. Shen, G. S. Denicol, B. Schenke, S. Jeon and C. Gale, “Importance of the Bulk Viscosity of QCD in Ultrarelativistic Heavy-Ion Collisions,” *Phys. Rev. Lett.* **115**, 132301 (2015).
- [27] B. I. Abelev *et al.* [STAR Collaboration], “Azimuthal Charged-Particle Correlations and Possible Local Strong Parity Violation,” *Phys. Rev. Lett.* **103**, 251601 (2009).
- [28] B. I. Abelev *et al.* [STAR Collaboration], “Observation of charge-dependent azimuthal correlations and possible local strong parity violation in heavy ion collisions,” *Phys. Rev. C* **81**, 054908 (2010).
- [29] D. Kharzeev, R. D. Pisarski and M. H. G. Tytgat, “Possibility of spontaneous parity violation in hot QCD,” *Phys. Rev. Lett.* **81**, 512 (1998).
- [30] D. Kharzeev, “Parity violation in hot QCD: Why it can happen, and how to look for it,” *Phys. Lett. B* **633**, 260 (2006).
- [31] S. A. Voloshin, “Parity violation in hot QCD: How to detect it,” *Phys. Rev. C* **70**, 057901 (2004).
- [32] STAR Collaboration, C. Adler *et al.*, *Nucl. Instr. Meth. A* **499**, 624 (2003).
- [33] A. Bilandzic, R. Snellings and S. Voloshin, “Flow analysis with cumulants: Direct calculations,” *Phys. Rev. C* **83**, 044913 (2011); A. Bilandzic, C. H. Christensen, K. Gulbrandsen, A. Hansen and Y. Zhou, “Generic framework for anisotropic flow analyses with multiparticle azimuthal correlations,” *Phys. Rev. C* **89**, 064904 (2014).
- [34] B. I. Abelev *et al.* [STAR Collaboration], “Systematic Measurements of Identified Particle Spectra in pp , d^+ Au and Au+Au Collisions from STAR,” *Phys. Rev. C* **79**, 034909 (2009).
- [35] M. L. Miller, K. Reygers, S. J. Sanders and P. Steinberg, “Glauber modeling in high energy nuclear collisions,” *Ann. Rev. Nucl. Part. Sci.* **57**, 205 (2007).
- [36] G. Aad *et al.* [ATLAS Collaboration], “Measurement of event-plane correlations in $\sqrt{s_{NN}} = 2.76$ TeV lead-lead collisions with the ATLAS detector,” *Phys. Rev. C* **90**, 024905 (2014).
- [37] M. Luzum and J. Y. Ollitrault, “Eliminating experimen-

- tal bias in anisotropic-flow measurements of high-energy nuclear collisions,” *Phys. Rev. C* **87**, 044907 (2013).
- [38] M. A. Lisa, S. Pratt, R. Soltz and U. Wiedemann, “Femtoscopy in relativistic heavy ion collisions,” *Ann. Rev. Nucl. Part. Sci.* **55**, 357 (2005).
- [39] Q. Y. Shou, Y. G. Ma, P. Sorensen, A. H. Tang, F. Videbk and H. Wang, “Parameterization of Deformed Nuclei for Glauber Modeling in Relativistic Heavy Ion Collisions,” *Phys. Lett. B* **749**, 215 (2015).
- [40] D. Teaney and L. Yan, “Non linearities in the harmonic spectrum of heavy ion collisions with ideal and viscous hydrodynamics,” *Phys. Rev. C* **86**, 044908 (2012).
- [41] L. Adamczyk *et al.* [STAR Collaboration], “Beam-energy dependence of charge separation along the magnetic field in Au+Au collisions at RHIC,” *Phys. Rev. Lett.* **113**, 052302 (2014).
- [42] STAR Collaboration, “Proposal for STAR TPC Inner Sector Upgrade (iTPC)”, STAR Note 0619: <https://drupal.star.bnl.gov/STAR/starnotes/public/sn0619>
- [43] K. H. Ackermann *et al.* [STAR Collaboration], “Elliptic flow in Au + Au collisions at $\sqrt{s_{NN}} = 130$ GeV,” *Phys. Rev. Lett.* **86**, 402 (2001); J. Adams *et al.* [STAR Collaboration], “Particle type dependence of azimuthal anisotropy and nuclear modification of particle production in Au + Au collisions at $\sqrt{s_{NN}} = 200$ GeV,” *Phys. Rev. Lett.* **92**, 052302 (2004); J. Adams *et al.* [STAR Collaboration], “Azimuthal anisotropy in Au + Au collisions at $\sqrt{s_{NN}} = 200$ GeV,” *Phys. Rev. C* **72**, 014904 (2005).
- [44] D. Molnar, “Novel mechanism of high- p_T production from an opaque quark-gluon plasma,” nucl-th/0503051.
- [45] short paper in preparation.
- [46] L. Adamczyk *et al.* [STAR Collaboration], “Fluctuations of charge separation perpendicular to the event plane and local parity violation in $\sqrt{s_{NN}} = 200$ GeV Au+Au collisions at the BNL Relativistic Heavy Ion Collider,” *Phys. Rev. C* **88**, no. 6, 064911 (2013).